https://doi.org/10.5194/essd-2026-603
Preprint. Discussion started: 20 August 2026

IrrEM (Irrigation in the eastern Mediterranean): Two and a half decades of seasonal high-resolution irrigated land maps of the eastern Mediterranean

Esmaeel Adrah[1], Luca Brocca[2], Emine Senkardesler[3], He Yin[1, 4, 5]

[1] Department of Geography, Kent State University, Kent, OH, USA
[2] Research Institute for Geo-Hydrological Protection, National Research Council, Perugia, Italy
[3] Department of Informatics, University of Illinois Urbana-Champaign, Champaign, IL, US
[4] School of Environment, Society & Sustainability, University of Utah, Salt Lake City, UT, USA
[5] Scientific Computing and Imaging Institute, University of Utah, Salt Lake City, UT, USA

Correspondence to:
Esmaeel Adrah (eadrah@kent.edu | esmaeelad@gmail.com)
He Yin (he.yin@utah.edu)

Abstract. Irrigation supports food security, drought resilience, and economic growth, but strains water resources and the environment. The eastern Mediterranean is a water-stressed region that relies heavily on agriculture. However, long-term irrigation patterns and their response to the regional challenges, such as frequent droughts and a war-torn agricultural system, remain poorly studied. NASA's satellite archive and recent remote sensing advancements offer an opportunity to fill this gap and support informed decision-making; however, adapting these tools to data-scarce regions and varying conditions remains a challenge. In this study, we present IrrEM (Irrigation in the eastern Mediterranean), which leverages the long-standing Landsat archive, a technique less reliant on training data, and cloud computing to map summer and winter irrigation extent at 30-m spatial resolution for the last 26 years in the eastern Mediterranean. We first processed each Landsat image into relative soil moisture using the Optical Trapezoid Model (OPTRAM). Next, we derived spatial and temporal irrigation indicators by tracking irrigation-induced changes of relative soil moisture across time and space, then used them to delineate irrigation extent. Evaluated against independent reference data, the maps achieved F-scores—the harmonic mean of precision and recall— ranging from 0.67 to 0.85. The open-access release comprises the annual summer and winter irrigation maps, ancillary layers (per-season counts of valid satellite observations and detected irrigation events), the OPTRAM parameters, the labelled reference data, the processing code, and an interactive web viewer (DOI: https://doi.org/10.5281/zenodo.17574601). Our study provides reproducible, timely, long-term, high-resolution irrigation maps for the eastern Mediterranean, freely available to support informed decisions, policy design, international aid, and further research in climate, agronomy, hydrology, and human-environment interaction.

1 Introduction

Irrigated areas account for 40% of global food production, yet 70% of global water withdrawals (Foley et al., 2011; McDermid et al., 2023; Mehta et al., 2024). Monitoring long-term spatial and temporal patterns of irrigation is essential for agricultural management (Mueller et al., 2017; Thiery et al., 2020), assessing water withdrawals (Peña-Arancibia et al., 2020; Rodell et al., 2018), energy consumption patterns (D'Odorico et al., 2018), food production patterns and their dynamics (Liu et al., 2017; Schultz

https://doi.org/10.5194/essd-2026-603
Preprint. Discussion started: 20 August 2026

et al., 2005), and socio-political dynamics (Dari et al., 2024a), especially in the context of climate change. However, information about irrigation areas remains difficult to obtain and is often unavailable in data-scarce regions, such as the eastern Mediterranean.

The eastern Mediterranean region is experiencing rapidly changing irrigation and food production patterns as water scarcity, prolonged droughts, displacement, conflict, and socio-political instability increasingly intersect. These pressures are particularly important in a region where agriculture depends heavily on limited and unevenly distributed water resources (Auda et al., 2024; FAO, 2021; Kaniewski et al., 2012; Li et al., 2022; Palatnik et al., 2025). Prolonged droughts and conflicts have further intensified this vulnerability (Atik et al., 2024; Müller et al., 2016), while geopolitical tensions over transboundary water resources complicate cooperative management efforts (FAO, 2009; Hasan et al., 2019). Despite the importance of irrigation for sustaining food production under these conditions, how these interacting challenges have reshaped the spatial and temporal patterns of irrigation remains poorly understood, largely due to the lack of reliable, long-term documentation on irrigation dynamics.

Despite the critical need for long-term high-resolution irrigation information across the eastern Mediterranean, existing datasets covering the region suffer from major limitations in spatial resolution, temporal frequency, geographic completeness, and mapping accuracy. Irrigation information is usually acquired from maps of areas equipped for irrigation, survey, remote sensing maps, or combined products. However, reliable irrigation data in the region remains critically limited; even when government records are available, they are often coarse, outdated, or of questionable accuracy (Auda et al., 2024; Fader et al., 2016; Kaniewski et al., 2012). The eastern Mediterranean is characterized by highly dynamic agricultural practices driven by seasonal water scarcity, interannual climate variability, shifting socio-political conditions, demographic changes, and displacement. As a result, irrigation patterns can change from season to season and across years, and information about area equipped for irrigation fail to capture these dynamics as they are updated infrequently and generally reflect single-year snapshots or intervals of several years to decades (Siebert et al., 2013).

Remote sensing offers cost-effective spatial and temporal coverage for the long-term monitoring of irrigation practices across diverse landscapes, effectively complementing traditional in situ methods (Ambika et al., 2016; Deines et al., 2019; Meier et al., 2018). However, existing maps in the eastern Mediterranean remain inadequate for delivering long-term, high-resolution data on irrigation dynamics for different set of challenges. Most available products are either global in scope or produced at coarse spatial resolutions (e.g., 250 m to several kilometers), limiting their ability to capture the region's spatial heterogeneity and temporal dynamics (Meier et al., 2018; Nagaraj et al., 2021; Salmon et al., 2015; Siebert et al., 2013). Although these datasets support large-scale assessments, their coarse resolution constrains applications requiring field-scale information (Velpuri et al., 2009; Xie et al., 2021). While high-resolution products has been developed to address this, the majority of high-resolution products covering the eastern Mediterranean are either a snapshot presenting only a single year (Van Tricht et al., 2023; Wu et al., 2023) or are geographically limited to individual basins or small study areas (Jaafar et al., 2015; Rufin et al., 2021). Additionally, even when irrigation products are available globally, they are often based on models predominantly trained on reference data from data-rich regions like the United States and Europe. As a result, they often fail to transfer to a new region such as the eastern Mediterranean, producing substantial classification errors across different heterogeneous geographies. For example, despite the overall satisfactory accuracy of the Landsat-Derived Global Rainfed and Irrigated-Cropland Product (LGRIP) and achieving high accuracy in the training region, it misclassifies the majority of rainfed agriculture in Syria and Turkey as irrigated, contradicting official statistics indicating that much of the cultivated land is rainfed (Teluguntla et al., 2023). Consequently, a critical need remains for high-resolution, temporally continuous irrigation records tailored to the eastern Mediterranean region.

Regional high-resolution irrigation datasets can be produced using remote sensing, helping overcome limitations associated with generalized, and coarse products. However, producing reliable maps for the eastern Mediterranean requires methods suited to data-scarce regions. Regional annual irrigation maps have been successfully developed for data-rich regions such as Europe, the United States, and China, where robust data availability supports such efforts. These approaches often rely on statistical and machine learning techniques to produce datasets such as CIrrMap250 (Zhang et al., 2024), LANID (Xie et al., 2021), IrrMapper (Ketchum et al., 2020), and regional maps for CONUS (Booth and Kucharik, 2025) and the High Plains Aquifer (Deines et al., 2019). While these methods often achieve high accuracy, they depend heavily on training data, and their applicability is typically limited to the regions where they were developed. As a result, data-scarce regions like the eastern Mediterranean require approaches that reduce reliance on extensive training data; however, such methods remain underutilized for irrigation monitoring in these areas.

Irrigation mapping approaches that rely less on training data have been developed by tracking the physical characteristics of vegetation or soil, particularly soil moisture. These soil-moisture-based methods overcome the challenges of data scarcity by focusing on physical irrigation indicators, enabling the dynamic mapping of irrigated areas without requiring extensive training datasets (Dari et al., 2021; Escorihuela and Quintana-Seguí, 2016; Kumar et al., 2015; Lawston et al., 2017; Le Page et al., 2020). While most of these studies rely on coarse-resolution satellite soil moisture products (Bazzi et al., 2022; Dari et al., 2024b), the need remains for a high-resolution irrigation mapping approach. Recently, there has been a growing interest in models for higher-resolution relative soil moisture estimates derived from optical sensors, such as the Optical Trapezoid Model (OPTRAM), leveraging the long historical record and relatively fine spatial and temporal resolutions of sensors such as Landsat and Sentinel-2 (Sadeghi et al., 2017).

This study leverages the OPTRAM model to estimate soil moisture from Landsat and utilize recent methodological development to produce high-resolution annual irrigation maps for the eastern Mediterranean. By reducing dependence on training data while exploiting the long historical record and fine spatial resolution of Landsat imagery, this work addressed a critical regional data gap and provides the long-term irrigation information needed to better understand agricultural change, water use, and regional water security under increasing climate and socio-political pressures.

2 Materials and methods

We employed a three-step framework to map irrigation extent across the eastern Mediterranean region (Fig. 1). First, we processed all available Landsat imagery covering the eastern Mediterranean region, including entire Syria, southern Turkey, and northern Jordan from 2000 to 2025 to derive relative soil moisture using the OPTRAM. Second, we utilized generated relative soil moisture dataset, in conjunction with rainfall data, to develop pixel-based irrigation indicators: (a) the artificial increases in relative soil moisture not attributable to rainfall, (b) the relative difference of soil moisture of the pixel of interest, and (c) the pixel's neighborhood change. Third, we applied these irrigation indicators to generate a binary map of irrigated versus non-irrigated areas. We then applied post-processing and masking to focus on agricultural land only. Finally, we evaluated the resulting maps using reference data, which included both existing datasets and manually collected samples.

We also used the Soil Moisture Active Passive Satellite mission (SMAP) to validate the calibration of OPTRAM-derived relative soil moisture. Additionally, we used rainfall data from Climate Hazards Group InfraRed Precipitation with Station data (CHIRPS) (Funk et al., 2015) to distinguish changes in relative soil moisture attributable to rainfall. To evaluate the accuracy of the final maps, we employed a combination of existing maps of the area equipped for irrigation and manually collected reference

https://doi.org/10.5194/essd-2026-603
Preprint. Discussion started: 20 August 2026

points. These reference points were obtained from interpreting high-resolution satellite imagery, ancillary data of irrigation infrastructure, and expert knowledge. Table 1 provides a summary of input datasets and their respective roles in map development. The following three sections detail the processing steps employed in this study.

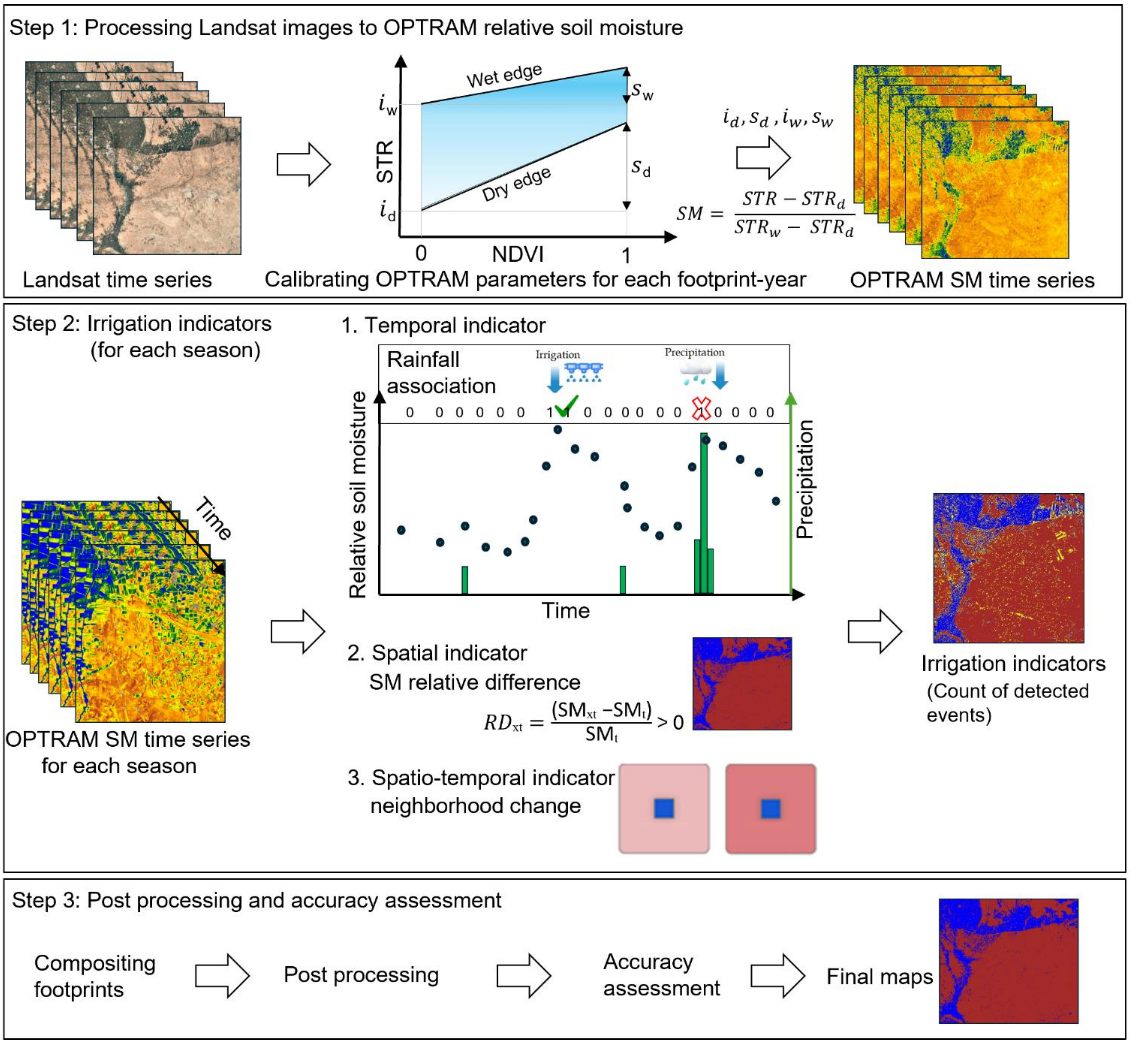

Figure 1: Overall methodology to produce seasonal irrigated land extent

https://doi.org/10.5194/essd-2026-603
Preprint. Discussion started: 20 August 2026

Table 1: Summary of input datasets

Data Type	Acquisition source	Resolution	Purpose
SWIR, Red, Blue bands	Landsat 5, 7, 8, 9	30 m	To derive relative soil moisture imagery, which is processed into annual irrigation indicators
Surface soil moisture	SMAP (Entekhabi et al., 2010)	9 km	To ensure proper calibration of the OPTRAM model and compare with the aggregated relative moisture as an intermediate quality control
Rainfall	Climate Hazards Group Infrared Precipitation with Station data (CHIRPS) (Funk et al., 2015).	5 km	To rule out the impact of rainfall events on relative soil moisture (8 days) when deriving irrigation indicators

2.1 Deriving OPTRAM relative soil moisture from Landsat imagery

The OPTRAM is grounded in the physical relationship between soil moisture and shortwave infrared transformed reflectance (STR), with its parameters derived from the distribution of pixels within the STR-Vegetation space (Sadeghi et al., 2017). This model was applied and tested to derive relative soil moisture for various applications and across different regions (Ambrosone et al., 2020; Longo-Minnolo et al., 2022; Mananze and Pôças, 2019; Mokhtari et al., 2023; Räsänen et al., 2022), including mapping irrigated area (Longo-Minnolo et al., 2022; Yao et al., 2022). The OPTRAM-derived relative soil moisture equation is as follows:

$$S = \frac{STR - STR_d}{STR_w - STR_d} = \frac{i_d + s_d\, NDVI - STR}{(i_d - i_w) + (s_d - s_w)\, NDVI} \qquad (1)$$

Where: S [m^3/m^3] is the soil moisture for each pixel, i_d, s_d [] are the parameters of the linear relationship between STR_d and Normalized Difference Vegetation Inde (NDVI) for dry edges ($STR_d = i_d + s_d\, NDVI$), i_w, s_w [] are the parameters of the linear relationship between STR_w and NDVI for wet edges ($STR_w = i_w + s_w\, NDVI$), STR [] is the short-wave infrared (SWIR) transformed reflectance ($STR = \frac{(1-SWIR)^2}{2*SWIR}$), NDVI [] is the normalized ratio between near-infrared (NIR) and red (RED) reflectance ($NDVI = \frac{NIR-RED}{NIR+RED}$).

An essential step in applying OPTRAM is defining the wet and dry edges to calibrate the model parameters (i_d, s_d, i_w, s_w). For calibration, we developed separate models for each Landsat footprint across a full year and tested three distinct calibration methods: (1) manual identification of wet and dry edges (Sadeghi et al., 2017), (2) adjusted parametrization based on SMAP data and land cover classification (Mohamadzadeh et al., 2025), and (3) linear fitting of NDVI-STR space for each scene over two years (Yao et al., 2022). We selected the third method based on an experimental comparison of the performance of each approach, using correlation and consistency between sampled Landsat images and SMAP soil moisture as a benchmark. Hence, we calibrated the model for each Landsat footprint by performing a linear fit in the NDVI–STR feature space for every footprint and each year. The calibration used Landsat observations from the current year together with data from the preceding year to ensure sufficient number of observations for linear fitting within Google Earth Engine (GEE). The resulting model parameters were generated for every Landsat footprint and year and are provided in the accompanying open-access data release.

As quality control of the calibration using linear fitting of NDVI-STR space, we compared the final output of OPTRAM and SMAP. To do so, we temporally matched each OPTRAM relative soil moisture image with the corresponding SMAP image

https://doi.org/10.5194/essd-2026-603
Preprint. Discussion started: 20 August 2026

and aggregated the OPTRAM pixels within each SMAP pixel using the mean value. Subsequently, we calculated Pearson's correlation coefficient (R) and root mean square error (RMSE) for each pair of matched Landsat imagery and SMAP. Because OPTRAM provides a measure of relative soil moisture and lacks a native physical scale, we linearly scaled the aggregated OPTRAM values to match the dynamic range of the SMAP observations. While this scaling is necessary to calculate RMSE, Pearson's correlation coefficient remains independent of this linear transformation. Given the known underestimation of soil moisture by SMAP (Fan et al., 2020), and the fact that OPTRAM estimates relative rather than absolute soil moisture lacking a meaningful physical scale, we focused the comparison on the correlation, which is the more relevant measure for our study's objective, as we are primarily using OPTRAM estimates as an indicator rather than as precise soil moisture values.

The OPTRAM-SMAP comparison was conducted for four Landsat footprints covering Landsat WRS Row 35 across four WRS Paths (171,172,173,174) covering our study areas' climate variability from the coastal area in the west to the inland dry area in the east. The comparison covered the full period of SMAP data availability, from 2015 to 2025 (Fig. A1-3). For the remaining footprints, and given the expensive computation required for this comparison, we sampled 50 random images from each remaining footprint and compared it to SMAP (Fig. A4).

2.2 Deriving temporal and spatial irrigation indicators

To distinguish between irrigated and non-irrigated land, we applied three criteria based on changes in OPTRAM relative soil moisture for each season. The temporal indicator identifies irrigation signals as artificial increases in soil moisture. To ensure that these increases are attributable to irrigation, we excluded any signals occurring within 8 days of rainfall events by integrating precipitation data. This temporal filtering helped to isolate irrigation-related moisture increases (Fig. 1-Step 2).

In addition to the temporal indicator, we employed a spatial-anomaly approach based on the temporal stability theory applied to irrigation mapping (Dari et al., 2021, 2024b, 2025). Using OPTRAM-derived relative soil moisture, we calculated the relative difference in soil moisture as an indicator for irrigation, under the assumption that irrigated areas typically exhibit higher average soil moisture compared to non-irrigated areas when no rainfall occurs. We used a conservative threshold of relative difference larger than zero as a qualifying criterion, rather than relying on optimized thresholds or clustering algorithms.

Next, we applied a spatio-temporal criteria that considered soil moisture changes in the neighborhood surrounding each pixel of interest. That is, in addition to the previous two criteria, a pixel was mapped as irrigated only when its soil moisture increased while the average soil moisture of its neighboring pixels decreased or stagnated. This criterion was designed to distinguish localized irrigation signals from broader moisture increases caused by regional environmental conditions. We tried a square neighborhood radius of 500, 1000, 1500, 2000, 2500, 3000, 3500, 4000, 4500, 5000, 10000 m. Because the resulting spatial patterns were stable for radius between 1000-5000 m, we hence we selected a radius of 2500 m to compute neighborhood-average soil moisture.

For each image, a pixel was labelled as irrigated only if it met the three above criteria in a given season. Given the rainy season and cropping patterns in the region, we considered two periods of analysis: winter irrigation from October to April, excluding December, January, and February) summer irrigation from May to September. We then counted the number of detected irrigation events within each season. A pixel in a seasonal map was classified as irrigated in a seasonable map if it had at least one irrigation event meeting during that season.

2.3 Post-processing

To address potential inconsistencies in irrigation detection caused by varying observation density, we applied a temporal smoothing based on the number of valid observations available for each pixel in each year. Smoothing was performed only for pixels with fewer valid observations than the 25th percentile of the observation distribution at that location (Fig. A6). We used a

https://doi.org/10.5194/essd-2026-603
Preprint. Discussion started: 20 August 2026

weighted five-year moving average, with weights proportional to the number of valid observations during the study season. This approach has significantly improved spatial consistency and reduced temporal gaps while having minimal effect on the final accuracy assessment (Fig. A7). We released both the original and temporally smoothed irrigation maps in the data release. Unless otherwise noted, all subsequent analyses were conducted using the smoothed dataset. To further reduce salt-and-pepper noise in the final irrigation maps while preserving larger, coherent irrigation patches, we applied an 8-pixel connected filter. We applied a 90 m square-kernel majority (mode) filter only to pixels belonging to small patches containing fewer than 50 connected pixels. Pixels within larger patches (≥50 connected pixels) retained their original classification. This conditional filtering limits smoothing to small, potentially spurious features while preserving the spatial integrity of larger irrigation areas, allowing contextual information from surrounding pixels to reduce noises, correct misclassified pixels, and consolidate fragmented regions (Hirayama et al., 2019).

2.4 Accuracy assessment

We followed established recommendations for assessing the accuracy of generated irrigation maps (Foody, 2009; Olofsson et al., 2013, 2014). Given the limited availability of reference data, we used manually collected reference samples supplemented by the datasets listed in Table 1. These reference samples were manually derived based on visual interpretation of very high-resolution imagery from Google Earth, in addition to utilizing ancillary datasets to infer irrigation status. We followed visual interpretation procedures from recent irrigation-extent validation frameworks (Dari et al., 2021; Deines et al., 2017, 2019; Xie et al., 2019, 2021; Xie and Lark, 2021; Zhang et al., 2024). Below, we detail the sampling design, response design, and analysis of our accuracy assessment.

Because irrigated areas exhibit substantial spatial heterogeneity, we used a stratified random sampling design to generate validation samples. We determined the sample size based on a planning value for the population proportion of 0.5, a target standard error of 0.05 for irrigated areas, and a 95% confidence level (Eq. 2) (Foody, 2009). This resulted in a desired sample of 400 pixels over 26 years.

$$n = \frac{Z^2 * p * (p-1)}{E^2} \qquad (2)$$

Where n is the desired sample size, Z is the level of confidence according to the standard normal distribution (z = 1.96 for 95% confidence); p is the population proportion, and E margin of error.

For the response design, we assigned validation labels by visually interpreting very high-resolution satellite imagery for each available year to determine whether a sample was irrigated or non-irrigated. These included inspecting greenness and crop growth during the dry season, contrast with surrounding fields, and textural patterns. We also inspected specific irrigation features such as preparation patterns for furrow irrigation (Fig. 2-a), center-pivot infrastructure (Fig. 2-b), filled or partially filled reservoirs (Fig. 2-c), proximity to canals and mapped irrigation infrastructure (Fig. 2-d), and correspondence with polygons of area equipped for irrigation and irrigation infrastructure network (Table 2). A validation label was assigned only when multiple independent lines of evidence supported the interpretation. In addition, seasonal NDVI profiles were reviewed before final labeling, and difficult cases were resolved in consultation with co-authors with regional expertise.

To maintain rigor and transparency of the labeling process while acknowledging the inherent uncertainty of labeling irrigation from imagery, we implemented a flexible reference labeling protocol. When visual interpretation confidence was low, samples were labeled as “uncertain,” and when no reliable conclusion could be drawn, an “N/A” label was assigned. Samples labeled as “N/A” were excluded from the quantitative accuracy assessment. Furthermore, years lacking suitable high-resolution imagery were removed from the reference set for the corresponding sample, reducing the final usable sample size to 2,528.

To ensure consistency among reference data collectors, all collectors were trained using a common interpretation protocol. In addition, each collector was assigned 25 randomly selected sample pixels that were also assigned to other collectors, enabling an assessment of inter-collector consistency. Each of these samples was independently labeled by two collectors. In cases of disagreement, an additional reviewer acted as a tiebreaker, either assigning the final label or making the point as "uncertain".

Finally, for each annual map, we constructed the error matrix and four accuracy metrics: Overall Accuracy (OA), Producer's Accuracy (PA), User's Accuracy (UA), and F1 score, calculated as $F1 = 2 \times UA \times PA/(UA + PA)$, which represents a harmonic mean of precision and recall. Additionally, we conducted and reported the analysis twice: once including the "uncertain" labels and once excluding them, considering only high-confidence data.

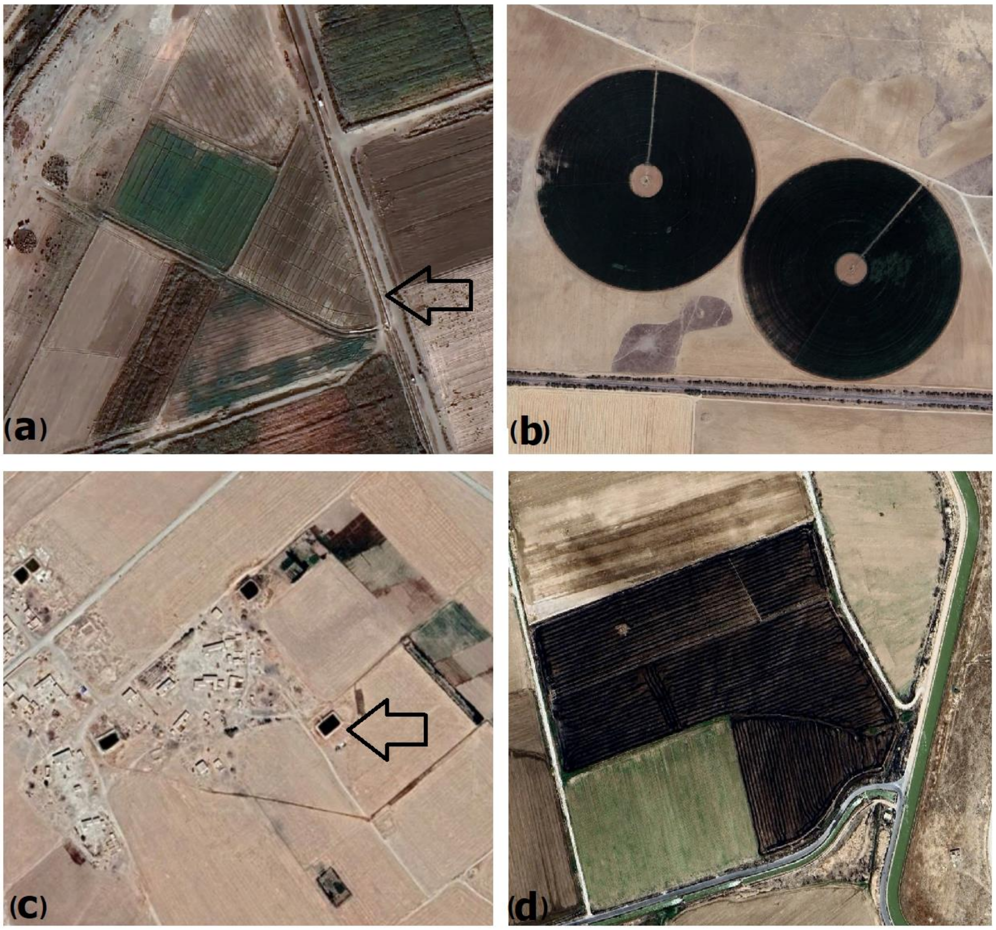

Figure 2 Examples of visual characteristics and spatial patterns used as indicators for labeling reference: a) furrow irrigation, b) pivot irrigation, c) field reservoir and management, d) proximity to canal and management. Sampling locations shown on satellite imagery from Google Earth. Image © 2025 Maxar Technologies, Image © 2025 CNES/Airbus accessed through Google Earth Pro

Table 2: Overview of auxiliary reference data and imagery sources evaluated during reference labeling.

Data Type	Acquisition source	Resolution
Maps of the area equipped for irrigation	Government agencies (FAO, 2008; Ministry of Agriculture and Forestry, 2025)	Vector data (Polygons)

https://doi.org/10.5194/essd-2026-603
Preprint. Discussion started: 20 August 2026

Data Type	Acquisition source	Resolution
Field and reference data from previous studies	(Kamkho, 2015)	Vector data (Points)
GRAIN: Irrigation infrastructure	(Suresh et al., 2025)	Vector data
GMIE: Global maximum irrigation extent and central pivot irrigation	(Tian et al., 2025)	100 m
High-resolution satellite images	Maxar, Worldveiw, Planet are available in Google Earth	0.2–3 m
NDVI time series	Landsat and Sentinel-2	10-30 m

3 Results

3.1 Parametrization of OPTRAM relative soil moisture

Our OPTRAM-derived relative soil moisture showed acceptable agreement with SMAP surface soil moisture across most Landsat footprints (Fig. 3, Fig A1-4). An average Pearson's correlation coefficient (R) of approximately 0.5 supports the application of OPTRAM as an indicator of relative, irrigation-driven soil moisture dynamics rather than a precise measure of absolute soil moisture magnitude. Notably, poor correlations (low R values) generally corresponded to images with extensive pixel masking due to clouds, shadows, or artifacts (Fig. A1). Nevertheless, spatial patterns remained consistent within the unmasked areas of these scenes (Fig. A1). The limitations associated with masked pixels and valid observations are mitigated through post-processing, detailed in Section 2.3 and discussed further in Section 4.2.2.

Visual inspections of OPTRAM-derived relative soil moisture showed that the model captured expected regional patterns, including realistic spatial gradients and coherent seasonal trajectories. The observed contrast between croplands and sparsely vegetated areas was consistent with known cropping patterns in the region (Fig. 3-c and 3-d). The spatial and temporal variability of OPTRAM outputs reflected differences in land cover, soil conditions, and closely followed regional irrigation and cropping cycles (Fig. A5).

Together, the correlation with SMAP, realistic land-cover-dependent spatial patterns, and coherent seasonal dynamics indicated that OPTRAM was appropriately parametrized for the study objective: detecting irrigation signals through anomaly tracking and the identification of artificial moisture increases (Fig. 3-a, 3-b, Fig. A1-4).

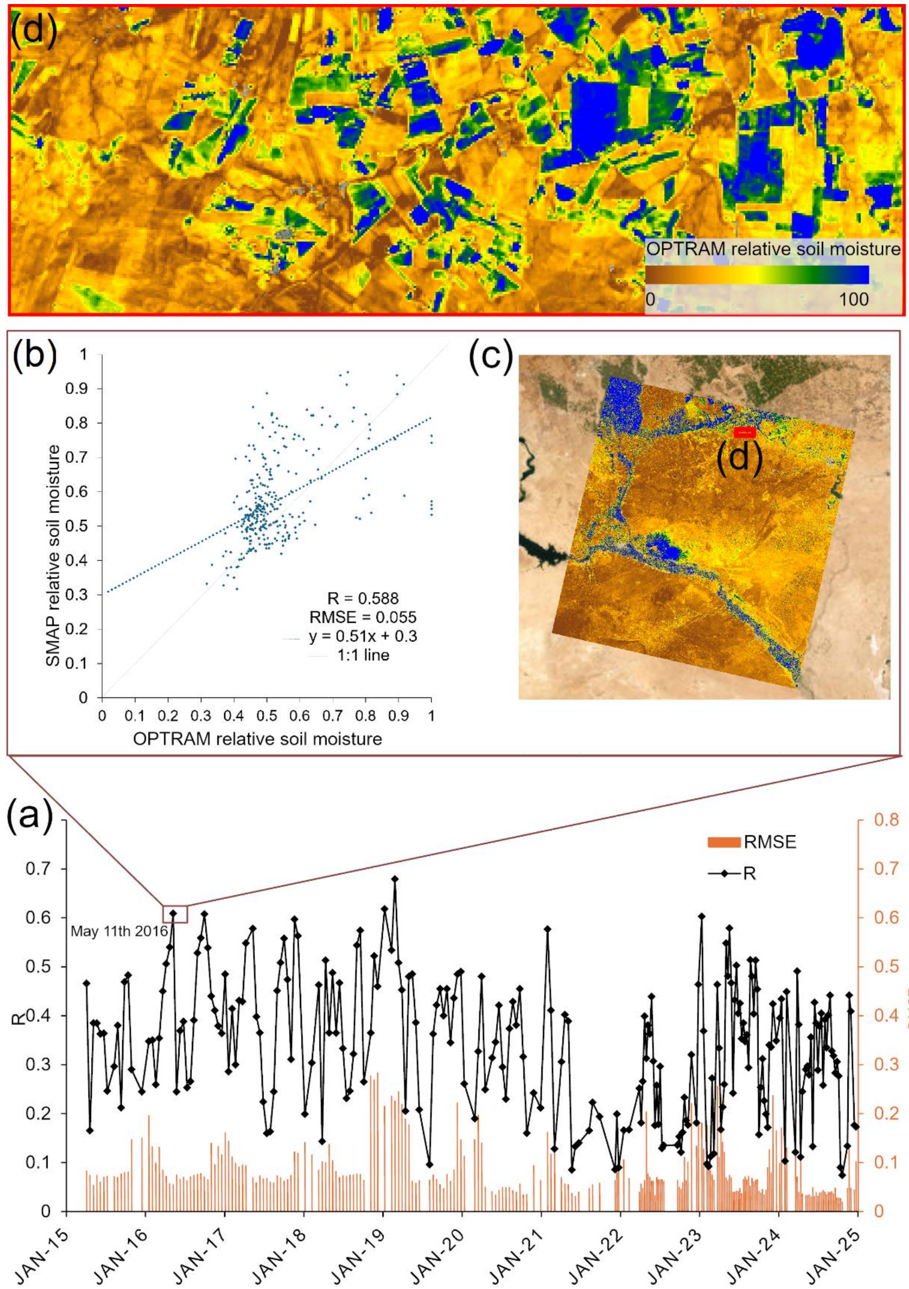

Figure 3 Comparison between SMAP and OPTRAM surface soil Moisture at the Landsat footprint. (a) Correlations and RMSE of all Landsat images between 2015 and 2025 (WRS path 172, WRS row 35). (b) Scatter plot of SMAP and OPTRAM for May 11th, 2016 (WRS path 172, WRS row 35). (c) OPTRAM relative soil moisture based on Landsat image (WRS path 172, WRS row 35), May 11, 2016. (d) Inset map of Landsat image processed to Relative soil moisture at 30 m resolution using OPTRAM.

3.2 Annual irrigation mapping

We generated annual summer and winter irrigation extent maps for the 2000–2025 period. To facilitate data exploration, the full 26-year time series of these maps is available to view and interact with via our online web application (https://water-middleeast.projects.earthengine.app/view/irrem). Across the 26-year record, the spatial distribution of detected irrigation aligns

https://doi.org/10.5194/essd-2026-603
Preprint. Discussion started: 20 August 2026

closely with known agricultural patterns and regions of intensive crop production (Fig. 4–5). High-productivity areas, such as river valleys and large-scale farming zones, consistently exhibited extensive irrigation coverage. Prominent examples include the Euphrates, Khabur, and Balikh River valleys across the northeastern Syrian governorates of Al-Hasakah, Ar-Raqqah, and Deir ez-Zor (Fig. 4a), as well as the Southeastern Anatolia (GAP) region in Türkiye (Fig. 4b). Conversely, mountainous terrains (e.g., coastal ranges) and remote arid zones (e.g., the Syrian Steppe and northern Jordan; Fig. 4c) displayed limited, fragmented irrigation, accurately reflecting regional water scarcity. Furthermore, barren terrains and desert environments outside established cropland boundaries (such as the Syrian Desert) were consistently classified as non-irrigated throughout the study period (Fig. 4–5).

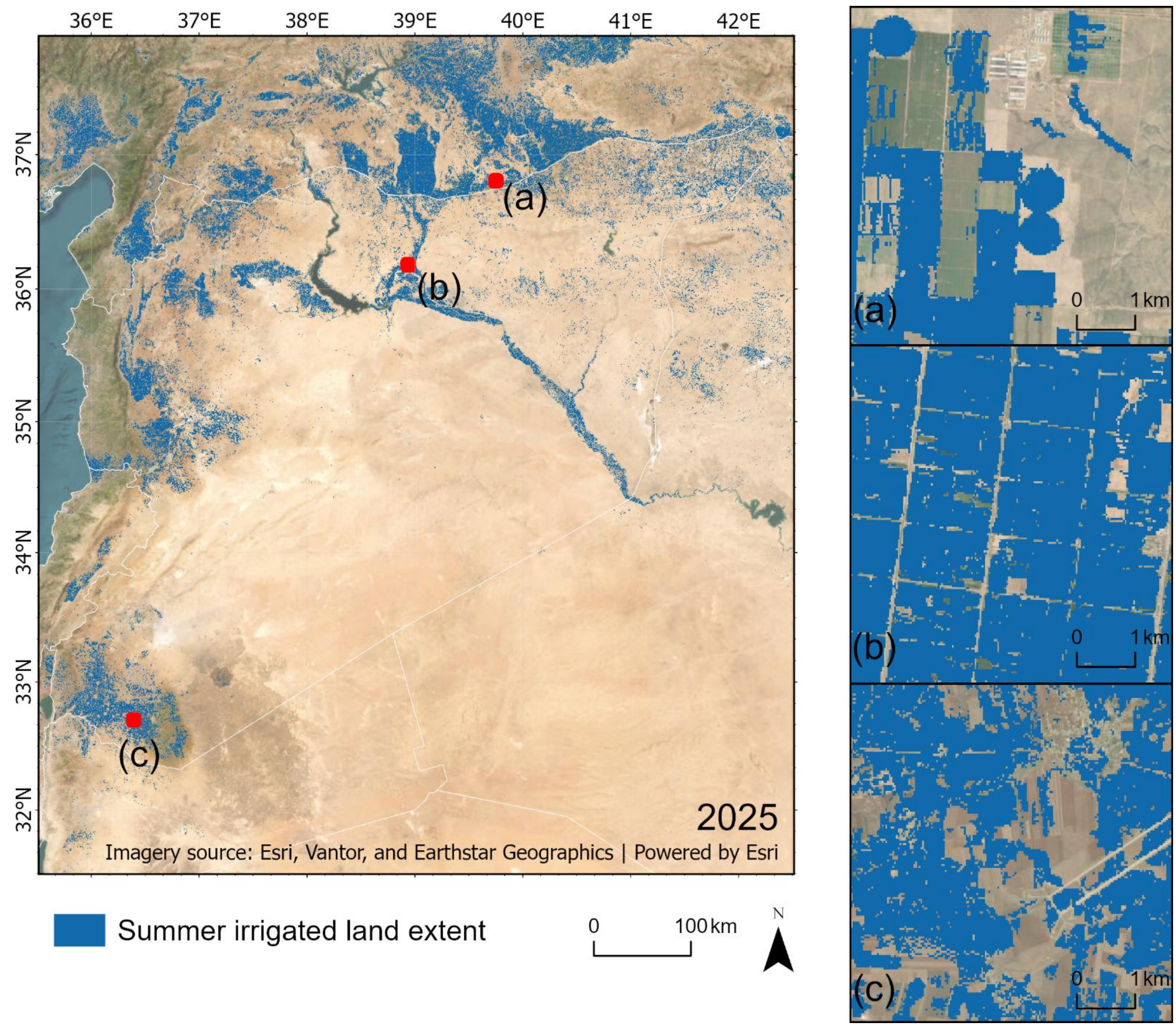

Figure 4 Example of mapped summer irrigated land extent in 2025. (a) pivot irrigation in the Southeastern Anatolia Region, often known as the GAP region, in Türkiye. (b) intensely irrigated area in Ar-Raqqah governorate along the Balikh River valleys in Syria (c) sparsely irrigated fields in semi-arid region southern Syria. The complete 26-year time series can be explored interactively at https://water-middleeast.projects.earthengine.app/view/irrem

In addition to broad regional consistency, the fine spatial detail afforded by our approach successfully captures field-scale irrigation patterns. The high-resolution maps delineate irrigation signals that align with individual agricultural fields, identifying characteristic geometries such as center pivots, block irrigation, and intensive valley farming (Fig. 4-5). This clear correspondence

https://doi.org/10.5194/essd-2026-603
Preprint. Discussion started: 20 August 2026

between mapped patterns and known field boundaries provides strong visual evidence that our method can isolate irrigation signals from natural background variability.

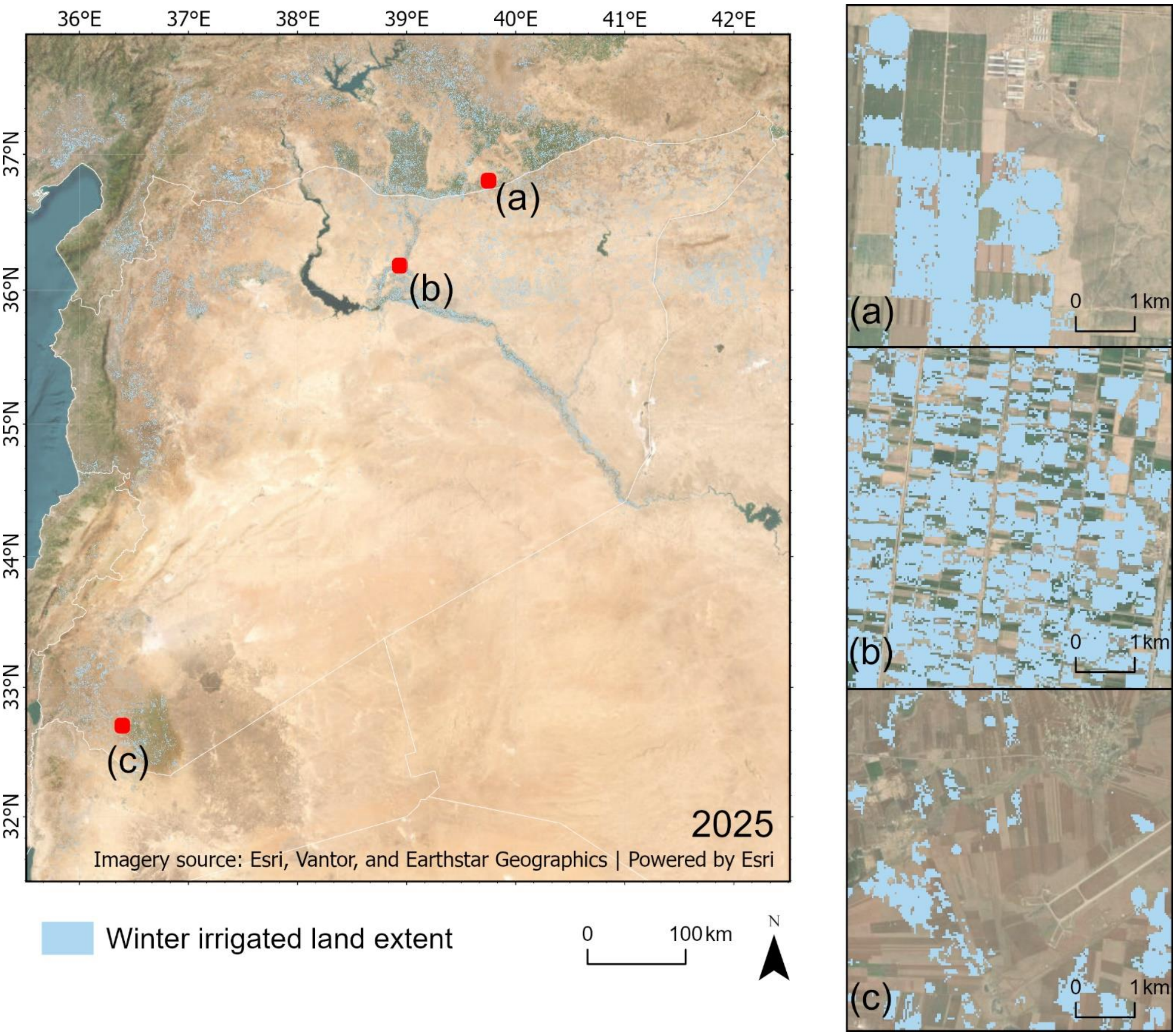

Figure 5 Example of mapped winter irrigated land extent in 2025. (a) pivot irrigation in the Southeastern Anatolia Region, often known as the GAP region, in Türkiye. (b) intensely irrigated area in Ar-Raqqah governorate along the Balikh River valleys in Syria (c) sparsely irrigated fields in semi-arid region southern Syria. The complete 26-year time series can be explored interactively at https://water-middleeast.projects.earthengine.app/view/irrem

Quantitative validation further contextualizes the model's performance, with overall accuracy ranging from 0.62 to 0.77 across the study period (Fig. 6). For the irrigated class, the F-score ranged from 0.67 to 0.85, and producer accuracy (PA) ranged from 0.74 to 0.92 (Fig. 7 and Fig. A8). These metrics demonstrate that the model successfully identifies the majority of true irrigated areas. However, temporal variations were evident: lower PA in certain years indicates occasional underestimation (omission errors) of actual irrigated land. Furthermore, user accuracy (UA) for the irrigated class ranged from 0.55 to 0.79. Although these metrics confirm that the majority of areas classified as irrigated correspond to true irrigation, they also reveal that commission errors remain a persistent source of uncertainty in specific years. The underlying causes of these misclassification,

https://doi.org/10.5194/essd-2026-603
Preprint. Discussion started: 20 August 2026

such as infrequent satellite overpasses, OPTRAM signal saturation during wet years, and other limitations, are addressed in detail in Section 4.3.

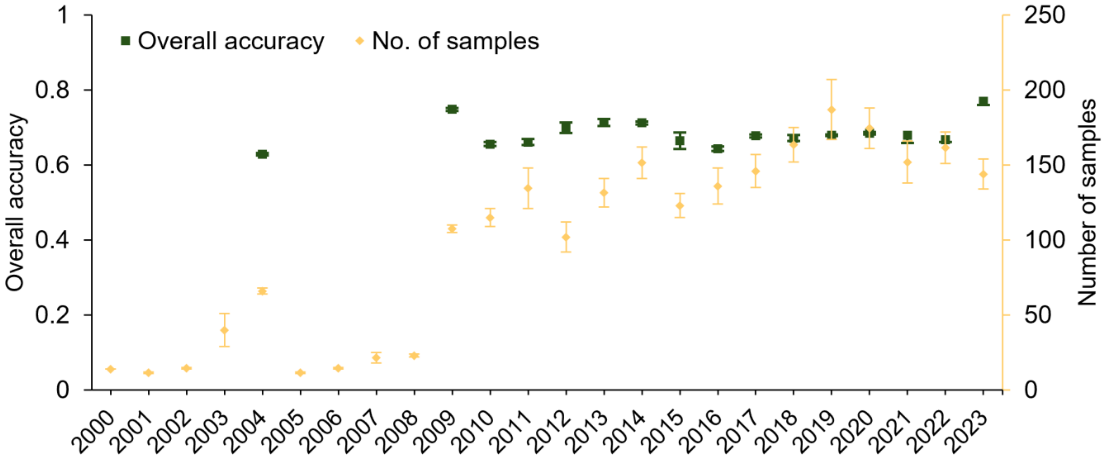

Figure 6 Overall accuracy and number of samples for each year. The error bars present the range of accuracy estimated using only high-confidence samples (upper bound) and the complete set of collected validation samples (lower bound).

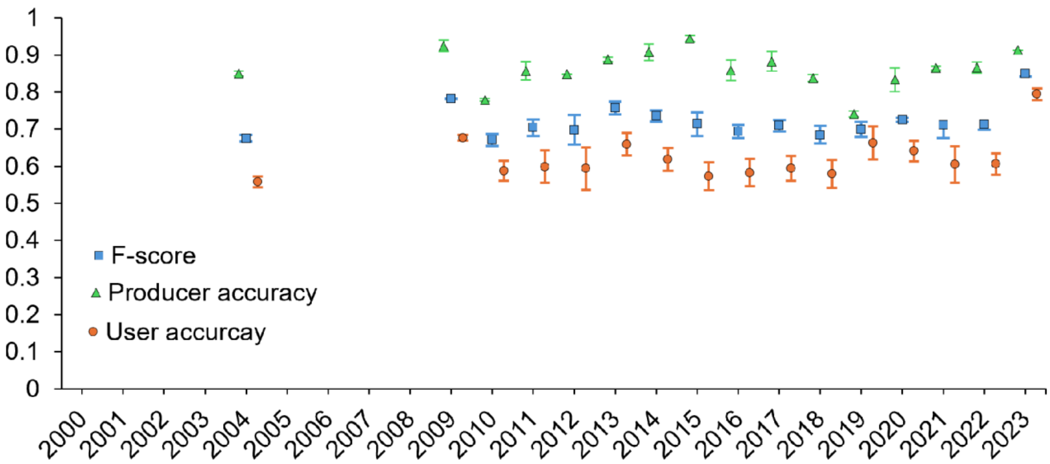

Figure 7 Irrigated F score, producer and user accuracy for each year. The error bars present the highest and lowest accuracy estimated using only high-confidence samples (upper bound) and the complete set of collected validation samples (lower bound).

4 Discussion

4.1 Comparison to existing irrigation products

Direct comparisons are limited since prior study provides long-term, high-resolution irrigation-extent maps with a formal accuracy assessment for the eastern Mediterranean are rare and global products historically underperform in the eastern Mediterranean. For example, despite the overall satisfactory accuracy globally, the global FAO WaPOR product achieved a producer's accuracy (PA) of just 15.9% when evaluated in Jordan's Amman–Zarqa basin (Al-Omoush et al., 2025), a stark contrast

https://doi.org/10.5194/essd-2026-603
Preprint. Discussion started: 20 August 2026

Open Access Earth System Science Data Discussions

to the regional PA of 0.74–0.92 achieved by IrrEM. Likewise, the Landsat-Derived Global Rainfed and Irrigated-Cropland Product (LGRIP) achieved high accuracy of approximately 90% globally and in the training region but misclassifies the entire rainfed areas in the eastern Mediterranean region as irrigated (Teluguntla et al., 2023). Furthermore, IrrEM's irrigated-class F-score (0.67–0.85) is highly competitive with state-of-the-art regional products, such as CIrrMap250 for China (F-score: 0.71–0.78; Zhang et al., 2024). While high-resolution models in the United States, such as LANID and IrrMapper, report overall accuracies exceeding 90% (Ketchum et al., 2020; Xie et al., 2021), these frameworks rely on dense, hand-labeled training datasets and pre-existing high-resolution cropland masks that do not exist for our study area. Our study delivers robust accuracy using a scalable approach that requires minimal training data and calibration. Despite a highly heterogeneous, cloud- and conflict-affected landscape, these metrics establish a reliable first baseline for long-term agricultural monitoring localized for the eastern Mediterranean.

4.2 Significance of the product and mapping approach

This study provides a significant contribution to agricultural and water resource monitoring in the eastern Mediterranean by addressing a long-standing gap in the availability of long-term, high-resolution irrigation extent data. Consistent monitoring of irrigation practices has historically been limited due to scarce ground reference information and a fragmented reporting system, particularly amid rapid environmental changes (Daher, 2022; World Bank, 2001), displacement (J. Wrathall et al., 2018; Müller et al., 2016), and conflict (Jaafar et al., 2015). By generating a continuous 26-year record of annual summer and winter irrigation extent at high spatial resolution, this work delivers a much-needed dataset capable of capturing continuous changes in irrigation over multiple decades. This level of detail is improvement compared to available data product in the eastern Mediterranean, which is essential for studies investigating irrigation changes and expanding its applications (Bazzi et al., 2022 Ketchum et al., 2020; Xie et al., 2021). Our dataset, therefore, provides a valuable foundation for understanding the underlying drivers of irrigation expansion or contraction in relation to conflict, environmental, and policy changes. It can also support research on agricultural adaptation, water allocation, transboundary water management, and resilience planning.

Methodologically, our approach reduces the reliance on reference data for irrigation map production and enables continuous updates of the irrigation maps. Our approach relies entirely on open-access satellite imagery and physically interpretable indicators of relative soil moisture changes, calibrated without reference data. By leveraging temporal and spatial signals associated with irrigation-induced moisture increases, our approach captures fine-scale irrigation signatures without requiring ground reference data typically required for model training, a critical advantage in the eastern Mediterranean, where such data is difficult to obtain and often historically unavailable. Similar physically based approaches have demonstrated strong performance in arid and semi-arid environments (Ambrosone et al., 2020; Dari et al., 2024b; Yao et al., 2022). Our findings are consistent with these results, further supporting the effectiveness of our approach for large-scale and long-term irrigation monitoring. Additionally, by making our code openly accessible, we enable continuous updates and refinement of the maps as new satellite data becomes available and support the adoption of the method by the research and practitioner communities.

In addition, our results highlight the effectiveness of our approach across diverse environmental settings and political boundaries. Turkey, Syria, and Jordan differ in climate, cropping systems, irrigation techniques, and water-management schemes, yet the framework was able to consistently capture irrigation extent across all three countries. This cross-boundary mapping capacity is particularly important in the eastern Mediterranean, where countries share and compete for transboundary water resources. Developing consistent irrigation maps across political boundaries can therefore provide a common evidence base for understanding regional water use, supporting comparative analysis, and informing cooperative water-resource management.

https://doi.org/10.5194/essd-2026-603
Preprint. Discussion started: 20 August 2026

4.3 Sources of uncertainties

While the dataset produced in this study provides valuable insight into the long-term changes of irrigation in the eastern Mediterranean, several uncertainties and limitations should be considered when interpreting the results or applying the maps.

4.3.1 Reference data limitations

Due to the scarcity of ground truth data in the eastern Mediterranean region, reference samples were mainly derived from interpreting very high-resolution satellite imagery and secondary sources. Although these approaches are widely used to compensate for the lack of historical reference data in irrigation mapping studies (Deines et al., 2017, 2019; Ketchum et al., 2020; Xie et al., 2019, 2021; Xie and Lark, 2021; Zhang et al., 2024), they introduce inherent uncertainties. For example, despite applying a rigorous framework for response design, distinguishing irrigated fields from non-irrigated fields from very high-resolution imagery remains challenging and subject to available visual clues and user interpretations, which may be ambiguous in certain periods, for small-scale or intermittent irrigation. We sought to account for these uncertainties through extensive label training and by assigning confidence levels throughout the labeling protocol; nevertheless, inherent interpretation errors remain unavoidable. Furthermore, secondary data that can aid the visual interpretation in the eastern Mediterranean region, such as crop type maps, is also limited or unreliable, which further hinders the interpretation process. Additionally, the spatial and temporal distribution of reference data is tied to high-resolution satellite imagery availability, which varies across time and region. As a result, in the absence of in situ ground truth, the ability to fine-tune the models across the region is hindered, and the accuracy estimates based on inferred reference data may contain bias linked to the reference data themselves. Comprehensive field-based validation campaigns would significantly strengthen future mapping efforts; however, such efforts remain difficult given the current constraints in the region.

4.3.2 Satellite revisit time

One source of uncertainty stems from the temporal resolution of Landsat imagery and inconsistency of cloud and shadow masking. Although Landsat offers an unparalleled long-term record, it’s effective revisit interval, typically 8 days under ideal conditions, considering data from at least two Landsat satellites in orbit. This interval is further limited due to cloud cover, sensor anomalies, and acquisition gaps. Irrigation-induced increase in surface soil moisture can dissipate within a few days, meaning that short-lived irrigation events may go undetected if they occur between satellite overpasses or during cloudy periods. To provide transparency regarding this limitation, our irrigation maps are accompanied by supplementary maps detailing the pixel-level count of valid observations for each year (Fig. 9A). Over the 2000–2025 study period, observation frequency exhibited significant seasonal and interannual variability with summer seasons yielded an average of 10 valid observations per pixel (range: 0–14), while winter seasons, which are shorter and more heavily impacted by cloud cover, averaged 4 valid observations per pixel (range: 0–7; Fig. 9A). Similar constraints were documented in other studies, which demonstrate that detecting irrigation becomes difficult when the time since irrigation exceeds 4 days, and that very rapid soil drying further necessitates high-temporal-frequency observations (Bazzi et al., 2020a; Le Page et al., 2020). This limitation may contribute to the underestimation of irrigated areas observed in years with lower producer accuracy. Although the issue cannot be fully eliminated, we applied methodological safeguards, such as stricter event detection criteria and flagging pixels with low temporal coverage that are temporally smoothed based on the weighted moving window explained in the method section (2.3), to help mitigate this issue. Future implementations

https://doi.org/10.5194/essd-2026-603
Preprint. Discussion started: 20 August 2026

could reduce this limitation by incorporating harmonized Landsat-Sentinel-2 imagery to improve temporal coverage for the post-2015 period.

4.3.3 OPTRAM and potential saturation

The OPTRAM-derived relative soil moisture patterns are reported to exhibit occurrences of saturated pixels (Mananze and Pôças, 2019; Sadeghi et al., 2017), the impact of this saturation in our maps, while minimal, can influence the accuracy especially in wet season. The relative soil moisture patterns observed in our maps exhibit expected spatial variability (Fig. 3c–d), and included limited occurrences of saturated pixels. Because our objective is to detect irrigation signals rather than absolute soil moisture retrieval, saturated pixels were treated conservatively: rain-associated pixels were masked, and only those consistent with expected irrigation timing and vegetation characteristics were retained. We also accounted for this issue during the calibration process by applying an NDVI upper threshold of 0.7 and masking forested areas when calculating the OPTRAM parameters, which further minimized the occurrence of saturated pixels. Nonetheless, in environments with persistent saturation, irrigation may still be misclassified because of saturated signals. Future enhancements could integrate the new variant of OPTRAM to account for this issue (Sadeghi et al., 2023).

4.3.4 Other sources of uncertainty

Interannual variability in the detectability of irrigation signals arises from shifts in crop planting dates, differences in irrigation frequency and intensity, inconsistent satellite coverage, and year-to-year variation in reference-data quality (Bazzi et al., 2020a; Massari et al., 2021). Several landscape and management characteristics also influence model sensitivity: crop-type differences in phenology and canopy structure can alter the visibility of irrigation-induced moisture signals (Bazzi et al., 2020b); irrigation methods such as drip systems generate subtler surface-moisture responses than sprinkler or flood irrigation (Hoque et al., 2025; Wang et al., 2000); soil and topographic conditions affect moisture retention, with permeable soils or sloped terrain leading to rapid drying (Bazzi et al., 2019). These factors were not explicitly accounted for in our maps due to the lack of field-based information on crop types, irrigation methods, and soil or management characteristics, data that remains scarce in the eastern Mediterranean and would require systematic ground observations.

4.4 Potential applications

The IrrEM maps provide critical spatial information for quantifying agricultural water use and supporting broader environmental modeling filling a long-standing gap in the eastern Mediterranean, where earlier irrigation datasets were either coarse or absent. By resolving active rather than equipped irrigation extent each year at 30 m over 26 years, the maps capture the maximum reach of irrigation and its year-to-year dynamics, including intermittently irrigated fields and land that has shifted between irrigated and rainfed use as conflict, drought, water availability, economics, and policy have changed. This makes them a foundation for research and management alike.

For water accounting, our maps supply the irrigated and non-irrigated delineation that pixel-level evapotranspiration (ET) products require before ET can be read as consumptive irrigation water use. Without accurate irrigation extent, regional irrigation rates and water-use fluxes cannot be reliably quantified. The dataset can also serve as input to climate and hydrological models, improving the representation of agricultural water use in simulations of water availability, groundwater recharge, surface runoff, and watershed-scale evapotranspiration (ET). In addition, it can support human–environment studies that examine the relationships between irrigation, soil quality, land productivity, and ecosystem services.

https://doi.org/10.5194/essd-2026-603
Preprint. Discussion started: 20 August 2026

The eastern Mediterranean is a focal point for research linking agriculture, water, and armed conflict, making IrrEM directly relevant to this literature. A prominent, unresolved debate concerns whether the severe 2006–2009 drought, and the subsequent agricultural collapse in northeastern Syria, triggered rural to urban migration and the onset of the 2011 civil war (Gleick, 2014; Kelley et al., 2015). Critics argue that the drought's extent and its causal link to migration were overstated, asserting that agricultural mismanagement and governance failures were the true drivers (de Châtel, 2014; Selby et al., 2017). Recent remote sensing evidence reframed this debate, indicating that Syrian agricultural activity recovered prior to the conflict, suggesting vulnerability is better explained by agricultural dynamics than by meteorology alone (Eklund et al., 2022). A recurring limitation across these studies, however, is the lack of long-term, spatially explicit records that separate irrigated from rainfed agriculture; existing analyses rely largely on vegetation greenness or cropland proxies that conflate the two. By providing a continuous, 30-m irrigation-specific record extending back to the pre-war period, IrrEM supplies the baseline needed to test these competing explanations and isolate climate-driven stress from management- and conflict-driven impacts.

Beyond climate-conflict debate, IrrEM supports the broader use of remote sensing to monitor conflict-driven agricultural change, expanding on approaches applied across Iraq, Syria, and Jordan (Eklund et al., 2017; Hazaymeh et al., 2022; Jaafar and Woertz, 2016; Yin et al., 2020). During regional conflicts, agricultural decline is driven not only by displacement but also by the withdrawal of subsidies and the disruption of water governance, which severely contracted irrigated schemes (Eklund et al., 2024; Li et al., 2022). Because IrrEM resolves irrigation temporally and spatially, it can help attribute such changes to their specific drivers, quantify productive capacity losses critical for humanitarian assessments, and document post-conflict recovery.

For decision-making, our maps can feed agricultural water-management systems to refine irrigation scheduling and reduce waste where water is limited, and they give policymakers a basis for targeting interventions, flagging zones of intense irrigation or over-extraction risk and tracking change over time to guide water allocation. Finally, in transboundary basins where the Euphrates and Tigris rivers are shared by Türkiye, Syria, and Iraq, and where water is contested (Gleick, 2019), transparent, cross-border data on active irrigation is critical. In a region of shared and contested water, transparent, open, high-resolution irrigation extents can support water diplomacy by directly inform assessments of water use and support the cooperative water management vital to regional stability.

5 Data availability

The irrigation data record is freely available at https://doi.org/10.5281/zenodo.17574601 (Adrah et al., 2025).
The dataset consists of the following primary categories:

- (Final) temporally smoothed irrigation extent for summer season and winter irrigation
- (Raw) Irrigation extent for summer season and winter irrigation
- Count of detected irrigation event for summer season and winter irrigation
- Number of valid satellite observation for summer season and winter irrigation
- OPTRAM Parameters: Contains the calculated wet/dry edge parameters for each Landsat footprint (Path/Row) per year
- Reference data used for Accuracy Assessment: Contains spatial coordinates, manually assigned ground-truth labels, and corresponding Landsat NDVI timeseries data used to validate the classification models.
- Interactive web app to view the final data product: https://water-middleeast.projects.earthengine.app/view/irrem

https://doi.org/10.5194/essd-2026-603
Preprint. Discussion started: 20 August 2026

Open Access Earth System Science Data Discussions

6 Code availability

The code developed for this study is openly available at https://github.com/Esmaeel-A/IrrEM_Irrigation-extent-mapping-without-training-data/. The repository includes all scripts used for preprocessing and irrigation detection.

7 Conclusion

This study addresses a critical gap in agricultural monitoring across the eastern Mediterranean by providing a continuous 26-year record of seasonal irrigation extents. By leveraging Landsat-derived soil moisture indicators, we successfully bypassed the need for the extensive ground training data typically required by conventional mapping methods, generating summer and winter irrigation maps at 30 m resolution annually. Evaluated against independent reference data, the maps achieved reliable F-scores of 0.67 to 0.85, establishing a robust baseline for analyzing long-term agricultural trends in a heavily data-scarce environment.

To ensure transparency and support reuse, we accompanied these maps with auxiliary layers detailing per-season detected irrigation events and valid satellite observations. Furthermore, we have released the complete dataset publicly, alongside the OPTRAM wet/dry-edge parameters for each Landsat footprint and year, the labeled reference data used for accuracy assessment, and the full processing code. An interactive web application also allows users to explore the final product directly.

The open dataset's relevance is sharpest where water is shared and contested: transparent, long-term irrigation data can ground transboundary allocation discussions in objective evidence and support water diplomacy, while also informing climate and hydrological modeling, water-resource management, and policy. While the absence of in situ ground truth for calibration and validation remains an inherent limitation in this setting, this study demonstrates that irrigation can be monitored effectively without extensive training data. Even in conflict-affected, data-scarce regions, this approach delivers the timely, high-resolution information required for land and water management as water scarcity and regional tensions intensify in the eastern Mediterranean.

https://doi.org/10.5194/essd-2026-603
Preprint. Discussion started: 20 August 2026

Appendix A

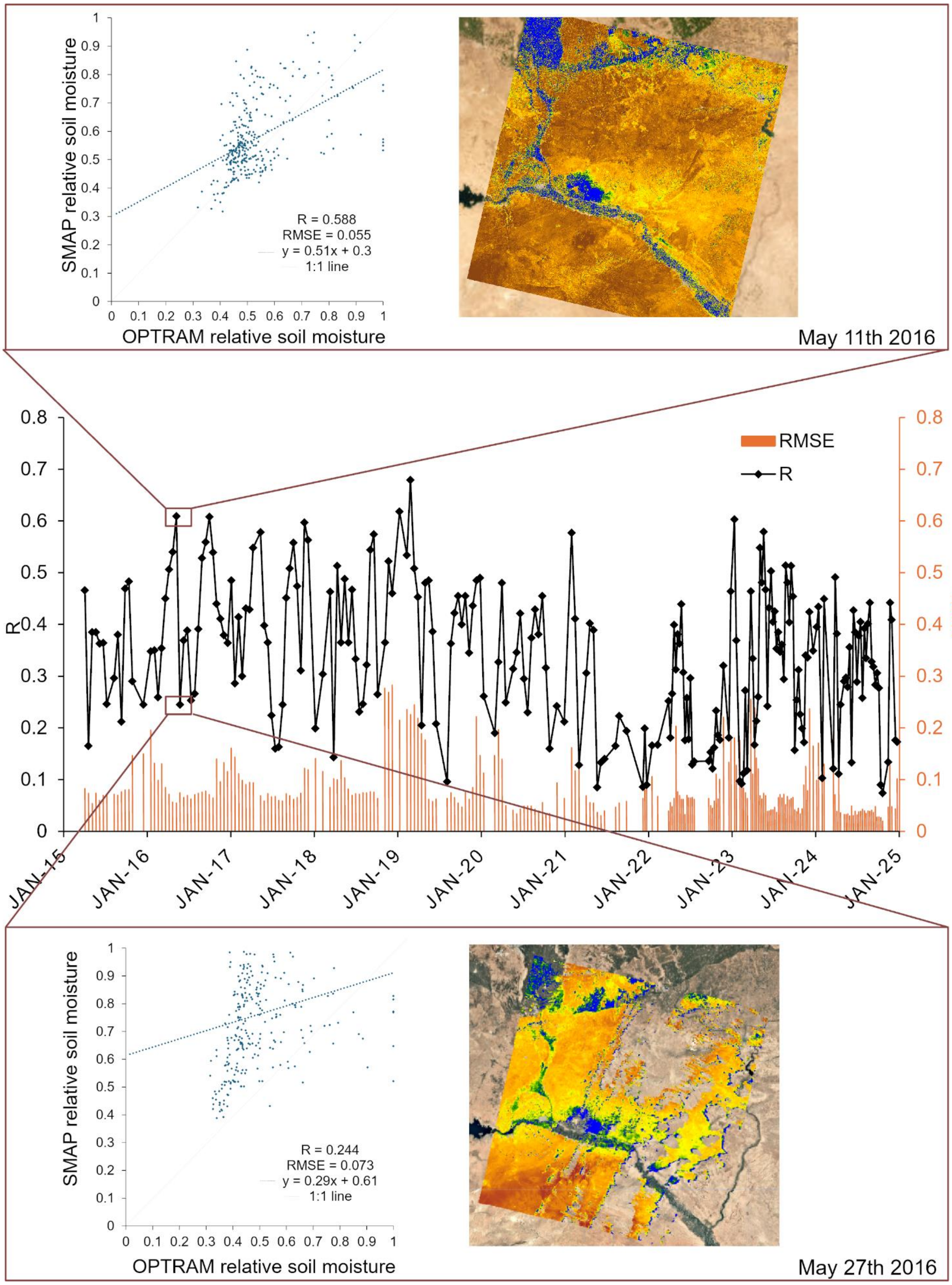

Fig. A1 Comparison between SMAP and OPTRAM surface soil Moisture at the Landsat footprint. Middle panel shows correlations and RMSE of all Landsat images between 2015 and 2025 (WRS path 172, WRS row 35). Upper panel shows a scatter plot of high correlation image between SMAP and OPTRAM for May 11th, 2016. Lower panel shows a scatter plot of low correlation image between SMAP and OPTRAM for May 27th, 2016.

https://doi.org/10.5194/essd-2026-603
Preprint. Discussion started: 20 August 2026

469

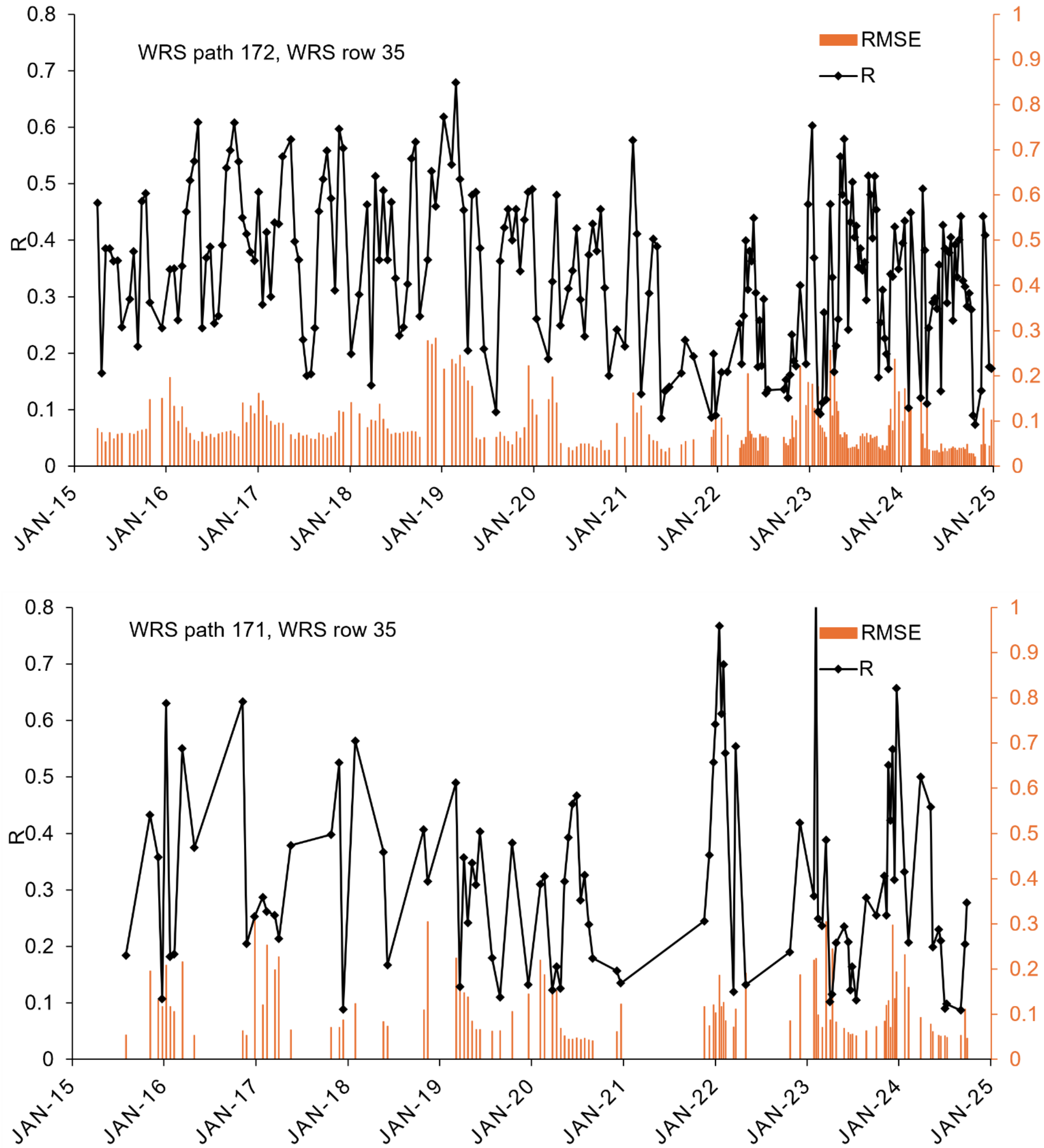

470
471 Fig. A2 Comparison between SMAP and OPTRAM surface soil Moisture at the Landsat footprint. Correlations and RMSE of
472 all Landsat images between 2015 and 2025 (WRS path 171, WRS row 35 and WRS path 172, WRS row 35).
473

https://doi.org/10.5194/essd-2026-603
Preprint. Discussion started: 20 August 2026

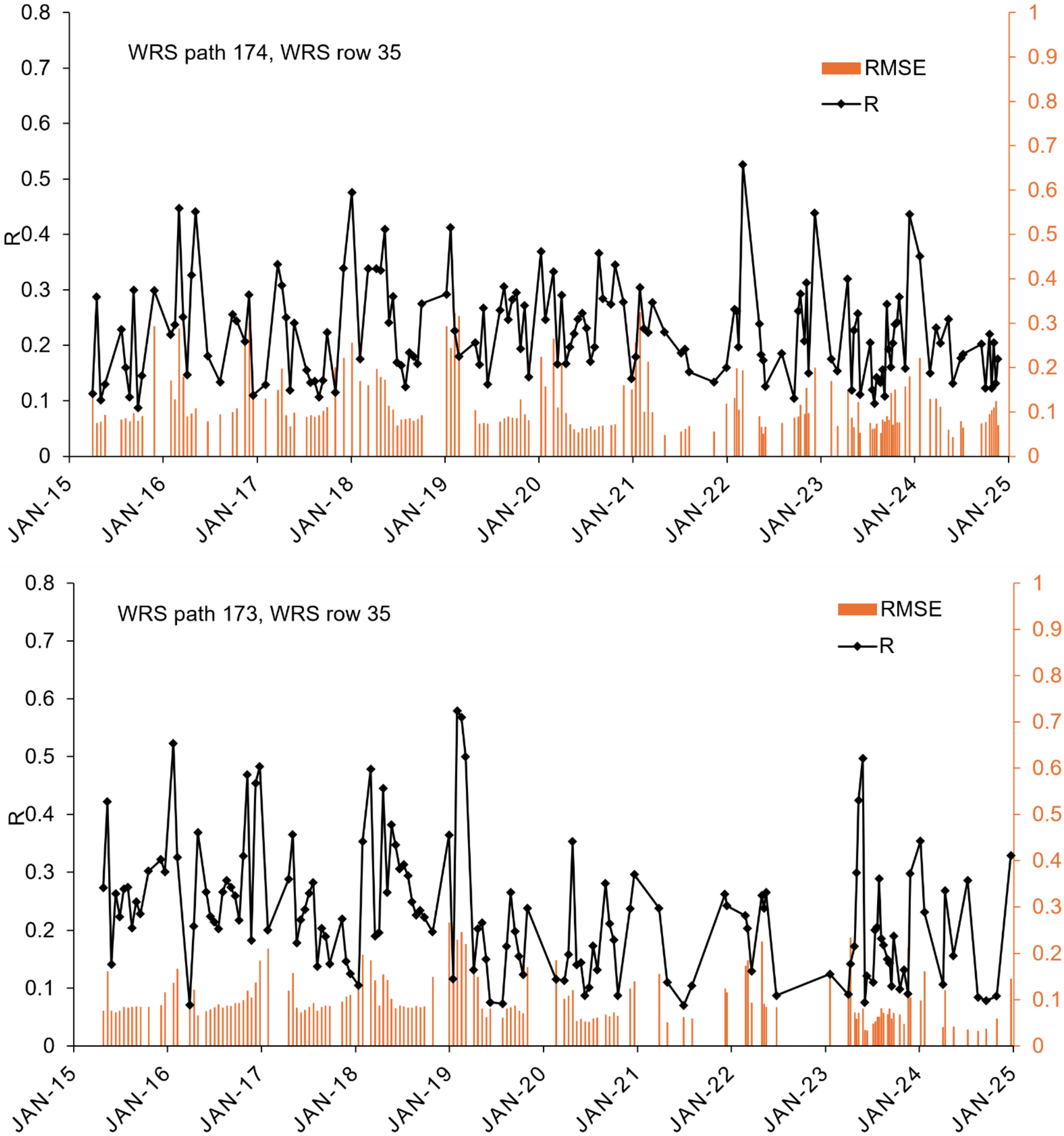

474
475 Fig. A3 Comparison between SMAP and OPTRAM surface soil Moisture at the Landsat footprint. Correlations and RMSE of
476 all Landsat images between 2015 and 2025 (WRS path 173, WRS row 35 and WRS path 174, WRS row 35).

Open Access Earth System Science Data Discussions

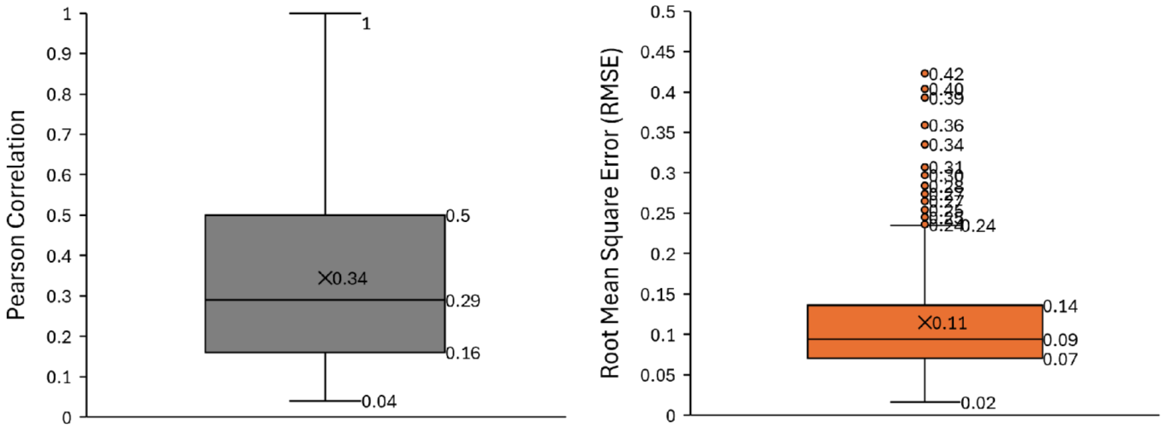

Fig. A4 Comparison between SMAP and OPTRAM surface soil Moisture at the Landsat footprint. Correlations and RMSE of stratified random samples of Landsat images between 2015 and 2025 across all WRS path and WRS rows covering the region (50 images each footprint).

https://doi.org/10.5194/essd-2026-603
Preprint. Discussion started: 20 August 2026

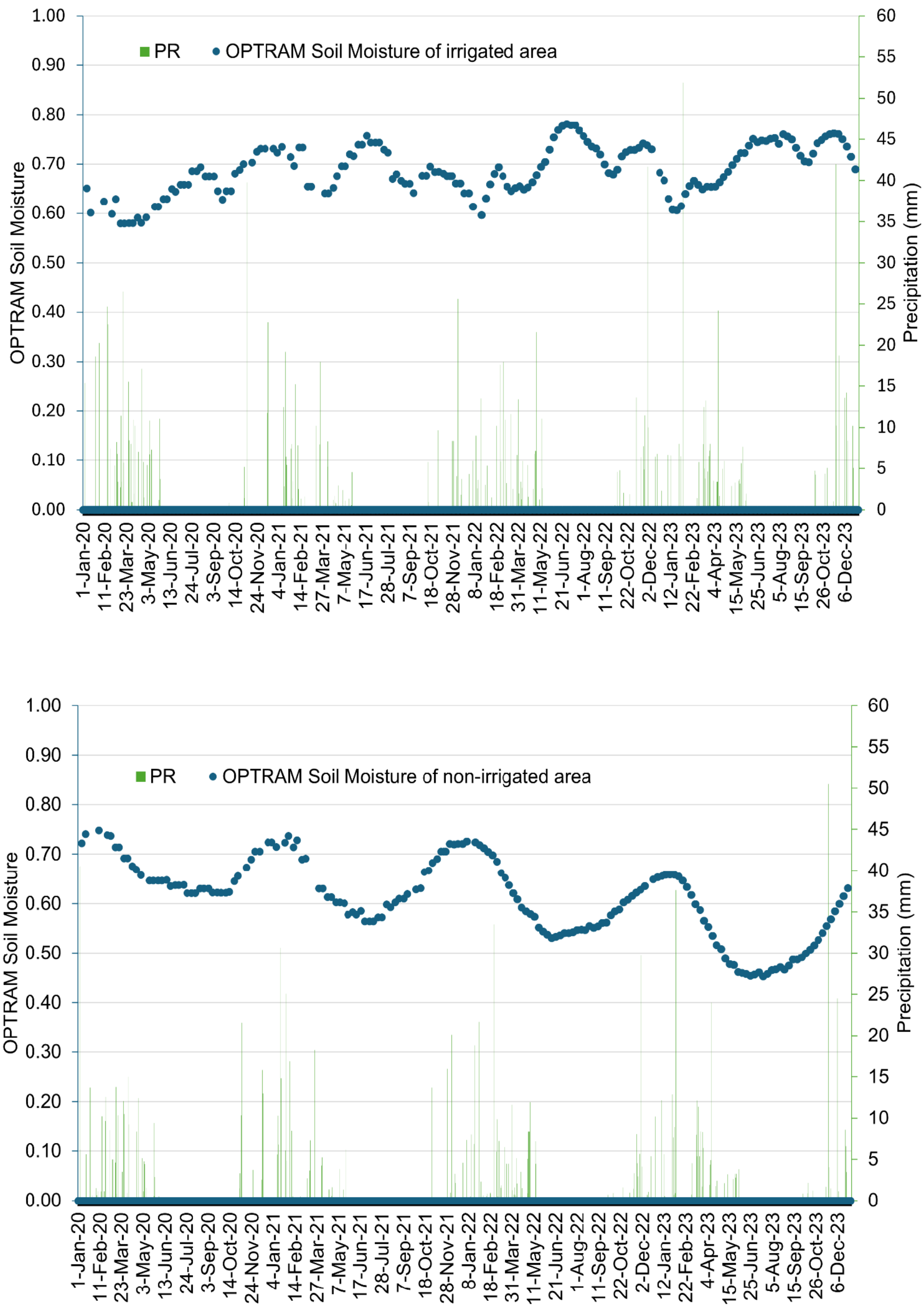

Fig. A5 OPTRAM Soil moisture response to rain and irrigation. Upper panel shows the response over irrigated areas. Lower panel shows the response over non-irrigated areas. (Note that OPTRAM was calibrated every year and hence year-to-year trends should not be interpreted from relative product).

https://doi.org/10.5194/essd-2026-603
Preprint. Discussion started: 20 August 2026

Open Access Earth System Science Data Discussions

Fig. A6 Weighted temporal smoothing. Only pixel-year with valid observations less than 25% percentile of the distribution of available observations for that location was smoothed. The smoothing process is conducted using a weighted moving average of 5 years window, where weights are the number of valid observations for each year during the studied season.

https://doi.org/10.5194/essd-2026-603
Preprint. Discussion started: 20 August 2026

Fig. A7 Comparison of final Irrigation map accuracy of raw data (unsmoothed) Vs. Temporally smoothed using 5 years weighted moving average window. Weights are determined by the total number of valid observations available for that year and total number of irrigation events detected for that year.

https://doi.org/10.5194/essd-2026-603
Preprint. Discussion started: 20 August 2026

Open Access Earth System Science Data Discussions

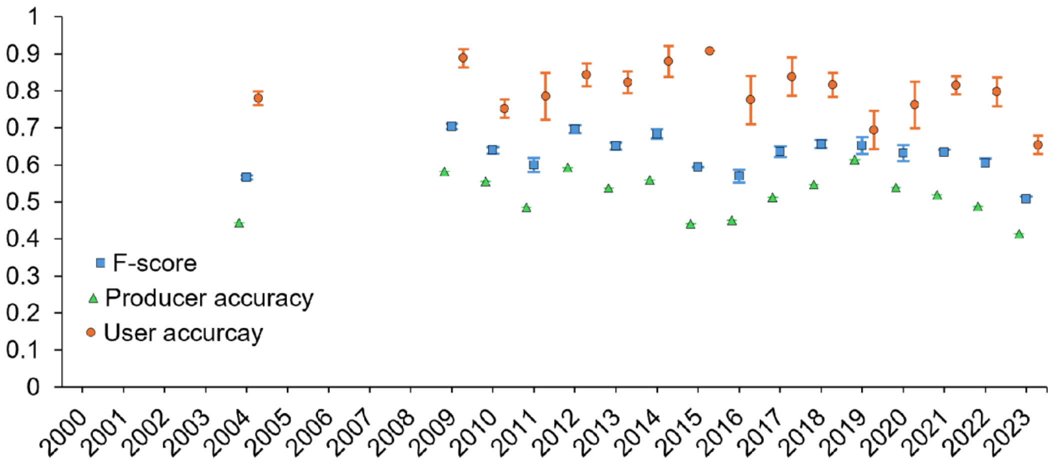

Fig. A8 Not-irrigated F score, producer and user accuracy for each year. The error bars show the highest and lowest accuracy estimated using only high-confidence samples (upper bound) and the complete set of collected validation samples (lower bound).

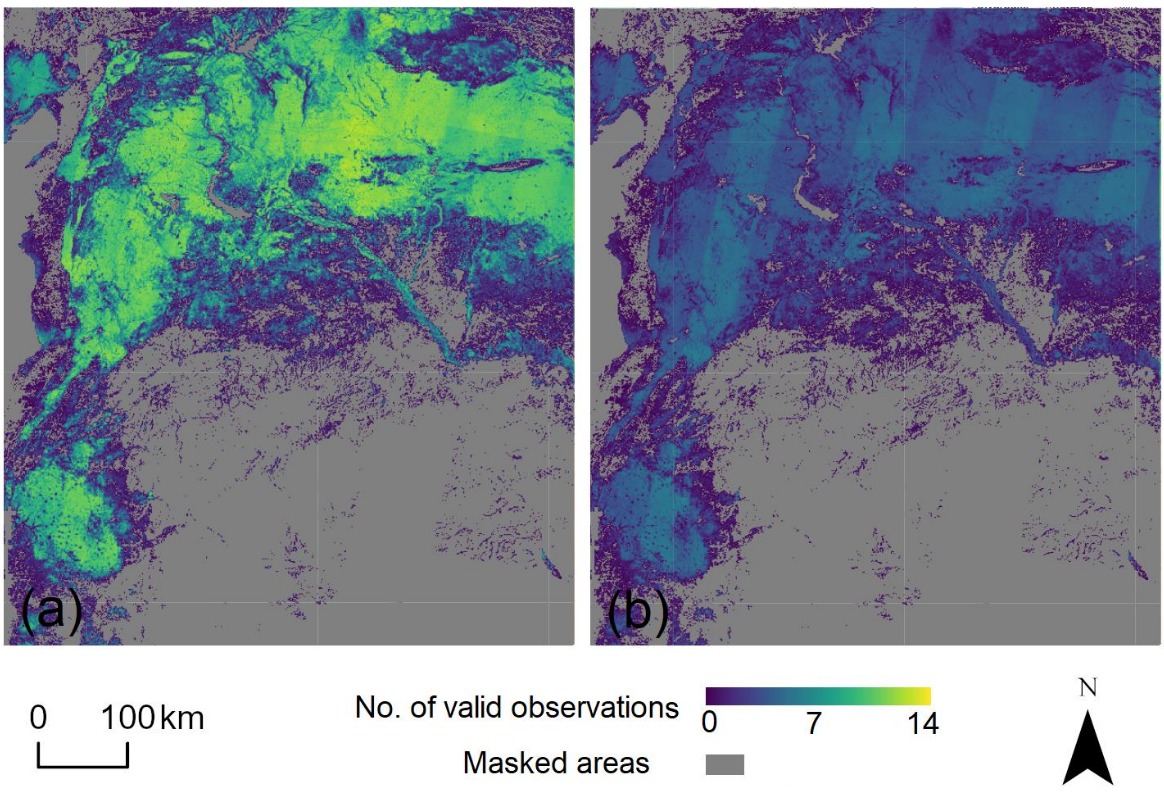

Fig. A9 Yearly average number of valid observations for the full study period (2000-2025) (a) summer (mean: 10, min: 0, max: 14) (b) winter (mean: 4, min:0, max: 7). Masked area is based on excluding Barren, Water and Built-up area using ESA World Colver V2.

https://doi.org/10.5194/essd-2026-603
Preprint. Discussion started: 20 August 2026

Author contributions

EA: conceptualization, methodology, software, validation, formal analysis, investigation, writing – original draft preparation, writing – review and editing, resources, data curation, visualization. HY: writing – review and editing, resources, investigation, supervision. LB: writing – review and editing, supervision. ES: writing – review and editing, data curation, validation.

Competing interests

The authors declare that they have no conflict of interest.

Acknowledgments

We gratefully acknowledge and thank Jackson Miller and Oliver Richard from Kent State University for assisting with reference data collection, and Sam Zipper from University of Kansas for earlier discussion. This work was supported by NASA (80NSSC21K0937) and this publication was made possible in part by support from the Kent State University Open Access Publishing. The authors express their sincere gratitude to the Water Diplomacy Center (WDC) at Jordan University of Science and Technology (JUST) for its financial support provided under the Blue Peace Middle East Capacity Development Project, funded by the Government of Switzerland.

Financial support

This publication was made possible in part by support from NASA New (Early Career) Investigator Program grant (80NSSC21K0937). This publication was made possible in part by support from the Kent State University Open Access Publishing. The authors express their sincere gratitude to the Water Diplomacy Center (WDC) at Jordan University of Science and Technology (JUST) for its financial support provided under the Blue Peace Middle East Capacity Development Project, funded by the Government of Switzerland.

Reference

Adrah, E., Brocca, L., Senkardesler, E., & Yin, H. (2026). Data — IrrEM (Irrigation in the eastern Mediterranean): Two and a half decades of seasonal high-resolution (30m) irrigated land maps of the eastern Mediterranean (2000-2025) [Dataset]. Zenodo. https://doi.org/10.5281/zenodo.17574601

Al-Omoush, R. A., Al-Bakri, J. T., Abdelal, Q., Al-Kilani, M. R., Hamdan, I., and Aljarrah, A.: Developing a remote sensing-based approach for agriculture water accounting in the Amman–Zarqa basin, Water, 17, 2106, https://doi.org/10.3390/w17142106, 2025.

Ambika, A. K., Wardlow, B., and Mishra, V.: Remotely sensed high resolution irrigated area mapping in India for 2000 to 2015, Sci. Data, 3, 160118, https://doi.org/10.1038/sdata.2016.118, 2016.

Ambrosone, M., Matese, A., Di Gennaro, S. F., Gioli, B., Tudoroiu, M., Genesio, L., Miglietta, F., Baronti, S., Maienza, A., Ungaro, F., and Toscano, P.: Retrieving soil moisture in rainfed and irrigated fields using Sentinel-2 observations and a modified OPTRAM approach, Int. J. Appl. Earth Obs. Geoinf., 89, 102113, https://doi.org/10.1016/j.jag.2020.102113, 2020.

Atik, O., Kadour, A., Mahmoud, I., Al Hasan, K., Al Nabhan, A., Jazieh, H., Nijhawan, A., and Pianosi, F.: Irrigation water in northwest Syria: impact of the recent crisis and drought, Water, 16, 3101, https://doi.org/10.3390/w16213101, 2024.

https://doi.org/10.5194/essd-2026-603
Preprint. Discussion started: 20 August 2026

Auda, A., Szilvácsku, Z. M., Bayot II, R., and Cuesta Tabares, M. A.: Water scarcity in Syria: the impact of the crisis on irrigated agriculture, Georgikon for Agriculture: A Multidisciplinary Journal in Agricultural Sciences, 2024.

Bazzi, H., Baghdadi, N., Ienco, D., El Hajj, M., Zribi, M., Belhouchette, H., Escorihuela, M. J., and Demarez, V.: Mapping irrigated areas using Sentinel-1 time series in Catalonia, Spain, Remote Sens., 11, 1836, https://doi.org/10.3390/rs11151836, 2019.

Bazzi, H., Baghdadi, N., Fayad, I., Charron, F., Zribi, M., and Belhouchette, H.: Irrigation events detection over intensively irrigated grassland plots using Sentinel-1 data, Remote Sens., 12, 4058, https://doi.org/10.3390/rs12244058, 2020a.

Bazzi, H., Baghdadi, N., Fayad, I., Zribi, M., Belhouchette, H., and Demarez, V.: Near real-time irrigation detection at plot scale using Sentinel-1 data, Remote Sens., 12, 1456, https://doi.org/10.3390/rs12091456, 2020b.

Bazzi, H., Baghdadi, N., and Zribi, M.: Comparative analysis between two operational irrigation mapping models over study sites in Mediterranean and semi-oceanic regions, Water, 14, 1341, https://doi.org/10.3390/w14091341, 2022.

Booth, E. G. and Kucharik, C. J.: Development of historical maps of land use-land cover, crop type, nutrients, and irrigation across CONUS (1938–2020) at different spatial resolutions, Earth Syst. Sci. Data, 18, 3415–3433, https://doi.org/10.5194/essd-18-3415-2026, 2026.

Chen, S., Huang, W., Chen, Y., and Feng, M.: An adaptive thresholding approach toward rapid flood coverage extraction from Sentinel-1 SAR imagery, Remote Sens., 13, 4899, https://doi.org/10.3390/rs13234899, 2021.

Chen, Z. and Zhao, S.: Automatic monitoring of surface water dynamics using Sentinel-1 and Sentinel-2 data with Google Earth Engine, Int. J. Appl. Earth Obs. Geoinf., 113, 103010, https://doi.org/10.1016/j.jag.2022.103010, 2022.

Daher, J.: Water scarcity, mismanagement, and pollution in Syria, European University Institute, https://hdl.handle.net/1814/74678, 2022.

Dari, J., Quintana-Seguí, P., Escorihuela, M. J., Stefan, V., Brocca, L., and Morbidelli, R.: Detecting and mapping irrigated areas in a Mediterranean environment by using remote sensing soil moisture and a land surface model, J. Hydrol., 596, 126129, https://doi.org/10.1016/j.jhydrol.2021.126129, 2021.

Dari, J., Filippucci, P., and Brocca, L.: The development of an operational system for estimating irrigation water use reveals socio-political dynamics in Ukraine, Hydrol. Earth Syst. Sci., 28, 2651–2659, https://doi.org/10.5194/hess-28-2651-2024, 2024a.

Dari, J., Morbidelli, R., Quintana-Seguí, P., and Brocca, L.: The temporal-stability-based irrigation MAPping (TSIMAP) method: a virtuous trade-off between accuracy, flexibility, and facility for end-users, Water, 16, 644, https://doi.org/10.3390/w16050644, 2024b.

Dari, J., Lo Presti, S., and Brocca, L.: Irrigation monitoring from satellite at hyper-high resolution: paving the way for remote-sensing-based agricultural water management support services, Agric. Water Manage., 317, 109627, https://doi.org/10.1016/j.agwat.2025.109627, 2025.

de Châtel, F.: The role of drought and climate change in the Syrian uprising: untangling the triggers of the revolution, Middle East. Stud., 50, 521–535, https://doi.org/10.1080/00263206.2013.850076, 2014.

Deines, J. M., Kendall, A. D., and Hyndman, D. W.: Annual irrigation dynamics in the U.S. Northern High Plains derived from Landsat satellite data, Geophys. Res. Lett., 44, 9350–9360, https://doi.org/10.1002/2017GL074071, 2017.

Deines, J. M., Kendall, A. D., Crowley, M. A., Rapp, J., Cardille, J. A., and Hyndman, D. W.: Mapping three decades of annual irrigation across the US High Plains Aquifer using Landsat and Google Earth Engine, Remote Sens. Environ., 233, 111400, https://doi.org/10.1016/j.rse.2019.111400, 2019.

D'Odorico, P., Davis, K. F., Rosa, L., Carr, J. A., Chiarelli, D., Dell'Angelo, J., Gephart, J., MacDonald, G. K., Seekell, D. A., Suweis, S., and Rulli, M. C.: The global food-energy-water nexus, Rev. Geophys., 56, 456–531, https://doi.org/10.1029/2017RG000591, 2018.

Eklund, L., Degerald, M., Brandt, M., Prishchepov, A. V., and Pilesjö, P.: How conflict affects land use: agricultural activity in areas seized by the Islamic State, Environ. Res. Lett., 12, 054004, https://doi.org/10.1088/1748-9326/aa673a, 2017.

Eklund, L., and Theisen, O. M.: Societal drought vulnerability and the Syrian climate-conflict nexus are better explained by agriculture than meteorology, Commun. Earth Environ., 3, 85, https://doi.org/10.1038/s43247-022-00405-w, 2022.

Eklund, L., Mohr, B., and Dinç, P.: Cropland abandonment in the context of drought, economic restructuring, and migration in northeast Syria, Environ. Res. Lett., 19, 014077, https://doi.org/10.1088/1748-9326/ad1723, 2024.

Entekhabi, D., Njoku, E. G., O'Neill, P. E., Kellogg, K. H., Crow, W. T., Edelstein, W. N., Entin, J. K., Goodman, S. D., Jackson, T. J., Johnson, J., Kimball, J., Piepmeier, J. R., Koster, R. D., Martin, N., McDonald, K. C., Moghaddam, M., Moran, S., Reichle, R., Shi, J. C., Spencer, M. W., Thurman, S. W., Tsang, L., and Van Zyl, J.: The Soil Moisture Active Passive (SMAP) mission, Proc. IEEE, 98, 704–716, https://doi.org/10.1109/JPROC.2010.2043918, 2010.

Escorihuela, M. J. and Quintana-Seguí, P.: Comparison of remote sensing and simulated soil moisture datasets in Mediterranean landscapes, Remote Sens. Environ., 180, 99–114, https://doi.org/10.1016/j.rse.2016.02.046, 2016.

Fader, M., Shi, S., von Bloh, W., Bondeau, A., and Cramer, W.: Mediterranean irrigation under climate change: more efficient irrigation needed to compensate for increases in irrigation water requirements, Hydrol. Earth Syst. Sci., 20, 953–973, https://doi.org/10.5194/hess-20-953-2016, 2016.

Fan, X., Liu, Y., Gan, G., and Wu, G.: SMAP underestimates soil moisture in vegetation-disturbed areas primarily as a result of biased surface temperature data, Remote Sens. Environ., 247, 111914, https://doi.org/10.1016/j.rse.2020.111914, 2020.

FAO: AQUASTAT Country Profile – Syrian Arab Republic, Food and Agriculture Organization of the United Nations (FAO), Rome, Italy, 2008.

FAO: AQUASTAT Transboundary River Basins – Euphrates-Tigris River Basin, Food and Agriculture Organization of the United Nations (FAO), Rome, Italy, 2009.

FAO: The impact of disasters and crises on agriculture and food security: 2021, Food and Agriculture Organization of the United Nations (FAO), Rome, Italy, https://doi.org/10.4060/cb3673en, 2021.

Foley, J. A., Ramankutty, N., Brauman, K. A., Cassidy, E. S., Gerber, J. S., Johnston, M., Mueller, N. D., O'Connell, C., Ray, D. K., West, P. C., Balzer, C., Bennett, E. M., Carpenter, S. R., Hill, J., Monfreda, C., Polasky, S., Rockström, J., Sheehan, J., Siebert, S., Tilman, D., and Zaks, D. P. M.: Solutions for a cultivated planet, Nature, 478, 337–342, https://doi.org/10.1038/nature10452, 2011.

Foody, G. M.: Sample size determination for image classification accuracy assessment and comparison, Int. J. Remote Sens., 30, 5273–5291, https://doi.org/10.1080/01431160903130937, 2009.

Gleick, P. H.: Water, drought, climate change, and conflict in Syria, Weather Clim. Soc., 6, 331–340, https://doi.org/10.1175/WCAS-D-13-00059.1, 2014.

Gleick, P. H.: Water as a weapon and casualty of armed conflict: a review of recent water-related violence in Iraq, Syria, and Yemen, WIREs Water, 6, e1351, https://doi.org/10.1002/wat2.1351, 2019.

Hasan, M., Moody, A., Benninger, L., and Hedlund, H.: How war, drought, and dam management impact water supply in the Tigris and Euphrates rivers, Ambio, 48, 264–279, https://doi.org/10.1007/s13280-018-1073-4, 2019.

Hazaymeh, K., Sahwan, W., Al Shogoor, S., and Schütt, B.: A remote sensing-based analysis of the impact of Syrian crisis on agricultural land abandonment in Yarmouk River basin, Sensors, 22, 3931, https://doi.org/10.3390/s22103931, 2022.

Hirayama, H., Sharma, R. C., Tomita, M., and Hara, K.: Evaluating multiple classifier system for the reduction of salt-and-pepper noise in the classification of very-high-resolution satellite images, Int. J. Remote Sens., 40, 2542–2557, https://doi.org/10.1080/01431161.2018.1528400, 2019.

Hoque, O. B., Mandal, N. C., Adiga, A., Swarup, S., Nouwakpo, S. K., Wilson, A., and Marathe, M.: Knowledge-informed deep learning for irrigation type mapping from remote sensing, in: Proceedings of the Thirty-Fourth International Joint Conference on Artificial Intelligence (IJCAI-25), https://doi.org/10.24963/ijcai.2025/1077, 2025.

Jaafar, H. H., Zurayk, R., King, C., Ahmad, F., and Al-Outa, R.: Impact of the Syrian conflict on irrigated agriculture in the Orontes basin, Int. J. Water Resour. D., 31, 436–449, https://doi.org/10.1080/07900627.2015.1023892, 2015.

Jaafar, H. H., and Woertz, E.: Agriculture as a funding source of ISIS: a GIS and remote sensing analysis, Food Policy, 64, 14–25, https://doi.org/10.1016/j.foodpol.2016.09.002, 2016.

Kamkho, M.: Mapping the agroecological zones (AEZs) in the Orontes River basin using remote sensing and geographic information systems (GIS) techniques, Ph.D. thesis, University of Aleppo, Syria, 2015.

Kaniewski, D., Van Campo, E., and Weiss, H.: Drought is a recurring challenge in the Middle East, Proc. Natl. Acad. Sci. U.S.A., 109, 3862–3867, https://doi.org/10.1073/pnas.1116304109, 2012.

Kelley, C. P., Mohtadi, S., Cane, M. A., Seager, R., and Kushnir, Y.: Climate change in the Fertile Crescent and implications of the recent Syrian drought, Proc. Natl. Acad. Sci. U.S.A., 112, 3241–3246, https://doi.org/10.1073/pnas.1421533112, 2015.

Ketchum, D., Jencso, K., Maneta, M. P., Melton, F., Jones, M. O., and Huntington, J.: IrrMapper: a machine learning approach for high resolution mapping of irrigated agriculture across the western U.S., Remote Sens., 12, 2328, https://doi.org/10.3390/rs12142328, 2020.

Kumar, S. V., Peters-Lidard, C. D., Santanello, J. A., Reichle, R. H., Draper, C. S., Koster, R. D., Nearing, G., and Jasinski, M. F.: Evaluating the utility of satellite soil moisture retrievals over irrigated areas and the ability of land data assimilation methods to correct for unmodeled processes, Hydrol. Earth Syst. Sci., 19, 4463–4478, https://doi.org/10.5194/hess-19-4463-2015, 2015.

Lawston, P. M., Santanello, J. A., and Kumar, S. V.: Irrigation signals detected from SMAP soil moisture retrievals, Geophys. Res. Lett., 44, 11860–11867, https://doi.org/10.1002/2017GL075733, 2017.

Le Page, M., Jarlan, L., El Hajj, M. M., Zribi, M., Baghdadi, N., and Boone, A.: Potential for the detection of irrigation events on maize plots using Sentinel-1 soil moisture products, Remote Sens., 12, 1621, https://doi.org/10.3390/rs12101621, 2020.

Li, X.-Y., Li, X., Fan, Z., Mi, L., Kandakji, T., Song, Z., Li, D., and Song, X.-P.: Civil war hinders crop production and threatens food security in Syria, Nat. Food, 3, 38–46, https://doi.org/10.1038/s43016-021-00432-4, 2022.

Liu, J., Hertel, T. W., Lammers, R. B., Prusevich, A., Baldos, U. L. C., Grogan, D. S., and Frolking, S.: Achieving sustainable irrigation water withdrawals: global impacts on food security and land use, Environ. Res. Lett., 12, 104009, https://doi.org/10.1088/1748-9326/aa88db, 2017.

Longo-Minnolo, G., Consoli, S., Vanella, D., Ramírez-Cuesta, J. M., Greimeister-Pfeil, I., Neuwirth, M., and Vuolo, F.: A stand-alone remote sensing approach based on the use of the optical trapezoid model for detecting the irrigated areas, Agric. Water Manage., 274, 107975, https://doi.org/10.1016/j.agwat.2022.107975, 2022.

Mananze, S. and Pôças, I.: Agricultural drought monitoring based on soil moisture derived from the optical trapezoid model in Mozambique, J. Appl. Remote Sens., 13, 024519, https://doi.org/10.1117/1.JRS.13.024519, 2019.

https://doi.org/10.5194/essd-2026-603
Preprint. Discussion started: 20 August 2026

Massari, C., Modanesi, S., Dari, J., Gruber, A., De Lannoy, G. J. M., Girotto, M., Quintana-Seguí, P., Le Page, M., Jarlan, L., Zribi, M., Ouaadi, N., Vreugdenhil, M., Zappa, L., Dorigo, W., Wagner, W., Brombacher, J., Pelgrum, H., Jaquot, P., Freeman, V., Volden, E., Fernandez Prieto, D., Tarpanelli, A., Barbetta, S., and Brocca, L.: A review of irrigation information retrievals from space and their utility for users, Remote Sens., 13, 4112, https://doi.org/10.3390/rs13204112, 2021.

McDermid, S., Nocco, M., Lawston-Parker, P., Keune, J., Pokhrel, Y., Jain, M., Jägermeyr, J., Brocca, L., Massari, C., Jones, A. D., Vahmani, P., Thiery, W., Yao, Y., Bell, A., Chen, L., Dorigo, W., Hanasaki, N., Jasechko, S., Lo, M.-H., Mahmood, R., Mishra, V., Mueller, N. D., Niyogi, D., Rabin, S. S., Sloat, L., Wada, Y., Zappa, L., Chen, F., Cook, B. I., Kim, H., Lombardozzi, D., Polcher, J., Ryu, D., Santanello, J., Satoh, Y., Seneviratne, S., Singh, D., and Yokohata, T.: Irrigation in the Earth system, Nat. Rev. Earth Environ., 4, 435–453, https://doi.org/10.1038/s43017-023-00438-5, 2023.

Mehta, P., Siebert, S., Kummu, M., Deng, Q., Ali, T., Marston, L., Xie, W., and Davis, K. F.: Half of twenty-first century global irrigation expansion has been in water-stressed regions, Nat. Water, 2, 254–261, https://doi.org/10.1038/s44221-024-00206-9, 2024.

Meier, J., Zabel, F., and Mauser, W.: A global approach to estimate irrigated areas – a comparison between different data and statistics, Hydrol. Earth Syst. Sci., 22, 1119–1133, https://doi.org/10.5194/hess-22-1119-2018, 2018.

Ministry of Agriculture and Forestry: Irrigated area 2025, General Directorate of State Hydraulic Works, DSI 15th Regional Directorate, Turkey, [dataset], 2025.

Mohamadzadeh, N., Sadeghi, M., Vergopolan, N., Liang, L., Bandara, U., Altare, C., and Caldas, M. M.: Landcover-specific calibration of the optical trapezoid model (OPTRAM) for soil moisture monitoring in the Central Valley, California, Front. Remote Sens., 6, 1519420, https://doi.org/10.3389/frsen.2025.1519420, 2025.

Mokhtari, A., Sadeghi, M., Afrasiabian, Y., and Yu, K.: OPTRAM-ET: a novel approach to remote sensing of actual evapotranspiration applied to Sentinel-2 and Landsat-8 observations, Remote Sens. Environ., 286, 113443, https://doi.org/10.1016/j.rse.2022.113443, 2023.

Mueller, N. D., Rhines, A., Butler, E. E., Ray, D. K., Siebert, S., Holbrook, N. M., and Huybers, P.: Global relationships between cropland intensification and summer temperature extremes over the last 50 years, J. Clim., 30, 7505–7528, https://doi.org/10.1175/JCLI-D-17-0096.1, 2017.

Müller, M. F., Yoon, J., Gorelick, S. M., Avisse, N., and Tilmant, A.: Impact of the Syrian refugee crisis on land use and transboundary freshwater resources, Proc. Natl. Acad. Sci. U.S.A., 113, 14932–14937, https://doi.org/10.1073/pnas.1614342113, 2016.

Nagaraj, D., Proust, E., Todeschini, A., Rulli, M. C., and D'Odorico, P.: A new dataset of global irrigation areas from 2001 to 2015, Adv. Water Resour., 152, 103910, https://doi.org/10.1016/j.advwatres.2021.103910, 2021.

Olofsson, P., Foody, G. M., Stehman, S. V., and Woodcock, C. E.: Making better use of accuracy data in land change studies: estimating accuracy and area and quantifying uncertainty using stratified estimation, Remote Sens. Environ., 129, 122–131, https://doi.org/10.1016/j.rse.2012.10.031, 2013.

Olofsson, P., Foody, G. M., Herold, M., Stehman, S. V., Woodcock, C. E., and Wulder, M. A.: Good practices for estimating area and assessing accuracy of land change, Remote Sens. Environ., 148, 42–57, https://doi.org/10.1016/j.rse.2014.02.015, 2014.

Palatnik, R. R., Raviv, O., Sirota, J., and Shechter, M.: Water scarcity and food security in the Mediterranean region: the role of alternative water sources and controlled-environment agriculture, Water Resour. Econ., 49, 100256, https://doi.org/10.1016/j.wre.2025.100256, 2025.

Peña-Arancibia, J. L., Mainuddin, M., Ahmad, M. D., Hodgson, G., Ibn Murad, K. F., Ticehurst, C., Maniruzzaman, M., Golam Mahboob, M., and Kirby, J. M.: Groundwater use and rapid irrigation expansion in a changing climate: hydrological drivers in one of the world's food bowls, J. Hydrol., 581, 124300, https://doi.org/10.1016/j.jhydrol.2019.124300, 2020.

Räsänen, A., Tolvanen, A., and Kareksela, S.: Monitoring peatland water table depth with optical and radar satellite imagery, Int. J. Appl. Earth Obs. Geoinf., 112, 102866, https://doi.org/10.1016/j.jag.2022.102866, 2022.

Rodell, M., Famiglietti, J. S., Wiese, D. N., Reager, J. T., Beaudoing, H. K., Landerer, F. W., and Lo, M.-H.: Emerging trends in global freshwater availability, Nature, 557, 651–659, https://doi.org/10.1038/s41586-018-0123-1, 2018.

Rufin, P., Müller, D., Schwieder, M., Pflugmacher, D., and Hostert, P.: Landsat time series reveal simultaneous expansion and intensification of irrigated dry season cropping in Southeastern Turkey, J. Land Use Sci., 16, 94–110, https://doi.org/10.1080/1747423X.2020.1858198, 2021.

Sadeghi, M., Babaeian, E., Tuller, M., and Jones, S. B.: The optical trapezoid model: a novel approach to remote sensing of soil moisture applied to Sentinel-2 and Landsat-8 observations, Remote Sens. Environ., 198, 52–68, https://doi.org/10.1016/j.rse.2017.05.041, 2017.

Sadeghi, M., Mohamadzadeh, N., Liang, L., Bandara, U., Caldas, M. M., and Hatch, T.: A new variant of the optical trapezoid model (OPTRAM) for remote sensing of soil moisture and water bodies, Sci. Remote Sens., 8, 100105, https://doi.org/10.1016/j.srs.2023.100105, 2023.

Salmon, J. M., Friedl, M. A., Frolking, S., Wisser, D., and Douglas, E. M.: Global rain-fed, irrigated, and paddy croplands: a new high resolution map derived from remote sensing, crop inventories and climate data, Int. J. Appl. Earth Obs. Geoinf., 38, 321–334, https://doi.org/10.1016/j.jag.2015.01.014, 2015.

Schultz, B., Thatte, C. D., and Labhsetwar, V. K.: Irrigation and drainage. Main contributors to global food production, Irrig. Drain., 54, 263–278, https://doi.org/10.1002/ird.170, 2005.

Selby, J., Dahi, O. S., Fröhlich, C., and Hulme, M.: Climate change and the Syrian civil war revisited, Polit. Geogr., 60, 232–244, https://doi.org/10.1016/j.polgeo.2017.05.007, 2017.

Siebert, S., Henrich, V., Frenken, K., and Burke, J.: Global Map of Irrigation Areas version 5 (5), Rheinische Friedrich-Wilhelms-University, Bonn, Germany / Food and Agriculture Organization of the United Nations, Rome, Italy, [dataset], 2013.

Stehman, S. V.: Estimating area from an accuracy assessment error matrix, Remote Sens. Environ., 132, 202–211, https://doi.org/10.1016/j.rse.2013.01.016, 2013.

Suresh, S., Hossain, F., Mishra, V., and Hossain, N.: GRAIN – a global registry of agricultural irrigation networks, Earth Syst. Sci. Data, 18, 1855–1870, https://doi.org/10.5194/essd-18-1855-2026, 2026.

Teluguntla, P., Thenkabail, P., Oliphant, A., Gumma, M., Aneece, I., Foley, D., and McCormick, R.: Landsat-derived global rainfed and irrigated-cropland product 30 m V001, NASA EOSDIS Land Processes DAAC, [dataset], https://doi.org/10.5067/COMMUNITY/LGRIP/LGRIP30.001, 2023.

Thiery, W., Visser, A. J., Fischer, E. M., Hauser, M., Hirsch, A. L., Lawrence, D. M., Lejeune, Q., Davin, E. L., and Seneviratne, S. I.: Warming of hot extremes alleviated by expanding irrigation, Nat. Commun., 11, 290, https://doi.org/10.1038/s41467-019-14075-4, 2020.

Tian, F., Wu, B., Zeng, H., Zhang, M., Zhu, W., Yan, N., Lu, Y., and Li, Y.: GMIE: a global maximum irrigation extent and central pivot irrigation system dataset derived via irrigation performance during drought stress and deep learning methods, Earth Syst. Sci. Data, 17, 855–880, https://doi.org/10.5194/essd-17-855-2025, 2025.

Tran, K. H., Menenti, M., and Jia, L.: Surface water mapping and flood monitoring in the Mekong Delta using Sentinel-1 SAR time series and Otsu threshold, Remote Sens., 14, 5721, https://doi.org/10.3390/rs14225721, 2022.

https://doi.org/10.5194/essd-2026-603
Preprint. Discussion started: 20 August 2026

Van Tricht, K., Degerickx, J., Gilliams, S., Zanaga, D., Battude, M., Grosu, A., Brombacher, J., Lesiv, M., Bayas, J. C. L., Karanam, S., Fritz, S., Becker-Reshef, I., Franch, B., Mollà-Bononad, B., Boogaard, H., Pratihast, A. K., Koetz, B., and Szantoi, Z.: WorldCereal: a dynamic open-source system for global-scale, seasonal, and reproducible crop and irrigation mapping, Earth Syst. Sci. Data, 15, 5491–5515, https://doi.org/10.5194/essd-15-5491-2023, 2023.

Velpuri, N. M., Thenkabail, P. S., Gumma, M. K., Biradar, C., Dheeravath, V., Noojipady, P., and Yuanjie, L.: Influence of resolution in irrigated area mapping and area estimation, Photogramm. Eng. Remote Sens., 75, 1383–1395, https://doi.org/10.14358/PERS.75.12.1383, 2009.

Wang, D., Shannon, M. C., Grieve, C. M., and Yates, S. R.: Soil water and temperature regimes in drip and sprinkler irrigation, and implications to soybean emergence, Agric. Water Manage., 43, 15–28, https://doi.org/10.1016/S0378-3774(99)00057-8, 2000.

World Bank: Syrian Arab Republic irrigation sector report, World Bank, Washington, D.C., Report No. 22602-SYR, 2001.

Wrathall, D. J., Van Den Hoek, J., Walters, A., and Devenish, A.: Water stress and human migration: a global, georeferenced review of empirical research, Food and Agriculture Organization of the United Nations (FAO), Rome, Italy, 2018.

Wu, B., Tian, F., Zhang, M., Piao, S., Zeng, H., Zhu, W., Liu, J., Elnashar, A., and Lu, Y.: Quantifying global agricultural water appropriation with data derived from earth observations, J. Clean. Prod., 358, 131891, https://doi.org/10.1016/j.jclepro.2022.131891, 2022.

Wu, B., Tian, F., Nabil, M., Bofana, J., Lu, Y., Elnashar, A., Beyene, A. N., Zhang, M., Zeng, H., and Zhu, W.: Mapping global maximum irrigation extent at 30m resolution using the irrigation performances under drought stress, Global Environ. Change, 79, 102652, https://doi.org/10.1016/j.gloenvcha.2023.102652, 2023.

Xie, Y. and Lark, T. J.: Mapping annual irrigation from Landsat imagery and environmental variables across the conterminous United States, Remote Sens. Environ., 260, 112445, https://doi.org/10.1016/j.rse.2021.112445, 2021.

Xie, Y., Lark, T. J., Brown, J. F., and Gibbs, H. K.: Mapping irrigated cropland extent across the conterminous United States at 30 m resolution using a semi-automatic training approach on Google Earth Engine, ISPRS J. Photogramm. Remote Sens., 155, 136–149, https://doi.org/10.1016/j.isprsjprs.2019.07.005, 2019.

Xie, Y., Gibbs, H. K., and Lark, T. J.: Landsat-based Irrigation Dataset (LANID): 30 m resolution maps of irrigation distribution, frequency, and change for the US, 1997–2017, Earth Syst. Sci. Data, 13, 5689–5710, https://doi.org/10.5194/essd-13-5689-2021, 2021.

Yao, Z., Cui, Y., Geng, X., Chen, X., and Li, S.: Mapping irrigated area at field scale based on the OPtical TRApezoid Model (OPTRAM) using Landsat images and Google Earth Engine, IEEE Trans. Geosci. Remote Sens., 60, 1–11, https://doi.org/10.1109/TGRS.2022.3148274, 2022.

Yin, H., Prishchepov, A. V., Kuemmerle, T., Bleyhl, B., Buchner, J., Radeloff, V. C., Baumann, M., Bragina, E. V., Kiel, A., and Schierhorn, F.: Monitoring cropland abandonment with Landsat time series, Remote Sens. Environ., 246, 111873, https://doi.org/10.1016/j.rse.2020.111873, 2020.

Zhang, L., Xie, Y., Zhu, X., Ma, Q., and Brocca, L.: CIrrMap250: annual maps of China's irrigated cropland from 2000 to 2020 developed through multisource data integration, Earth Syst. Sci. Data, 16, 5207–5226, https://doi.org/10.5194/essd-16-5207-2024, 2024.